

# Coupled Maxwell-pseudospin equations for investigation of self-induced transparency effects in a degenerate three-level quantum system in two dimensions: Finite-difference time-domain study

G. Slavcheva, J. M. Arnold, I. Wallace, and R. W. Ziolkowski\*

*Department of Electronics and Electrical Engineering, University of Glasgow, Glasgow G12 8QQ, United Kingdom*

(Received 7 March 2002; revised manuscript received 24 August 2002; published 31 December 2002)

We extend to more than one spatial dimension the semiclassical full-wave vector Maxwell-Bloch equations for the purpose of achieving an adequate and rigorous description of ultrashort pulse propagation in optical waveguides containing resonant nonlinearities. Our considerations are based on the generalized pseudospin formalism introduced by Hioe and Eberly [Phys. Rev. Lett. **47**, 838 (1981)] for treatment of the resonant coherent interactions of ultrashort light pulses with discrete-multilevel systems. A self-consistent set of coupled curl Maxwell-pseudospin equations in two spatial dimensions and time for the special case of a degenerate three-level system of quantum absorbers is originally derived. Maxwell's curl equations are considered to be coupled via macroscopic medium polarization to the three-level atom model for the resonant medium. Two distinct sets of pseudospin equations are obtained corresponding to the TE- and TM-polarized optical waves. For the case of TM polarization, the electromagnetic wave is polarized in a general direction in the plane of incidence inducing two dipole transitions in a degenerate three-level system by each  $E$ -field component along the propagation axis and in transverse direction. We introduce a dipole-coupling interaction Hamiltonian allowing Rabi flopping of the population difference along and perpendicular to the propagation axis with frequencies depending on the corresponding field components. The relationship between the induced polarization and the state vector components that describe the evolution of the discrete-level system is derived in order to couple the quantum system equations to the Maxwell's curl equations. The pseudospin equations are phenomenologically extended to include relaxation effects by introducing nonuniform decay times corresponding to the various dipole transitions occurring in a three-level system. The system has been discretized using finite differences on a Yee grid and solved numerically by an iterative predictor-corrector finite-difference time-domain method. Self-induced transparency soliton propagation through a degenerate three-level quantum system of absorbers in two spatial dimensions and time is demonstrated in planar parallel-mirror waveguide geometries.

DOI: 10.1103/PhysRevA.66.063418

PACS number(s): 42.50.Md, 42.65.Tg, 42.81.Dp, 42.50.Ct

## I. INTRODUCTION

State-of-the-art high-speed optical communications are constantly pushing further the demands for the generation of ultrashort light pulses. Recently, substantial progress has been achieved in the methods of generating extremely short optical pulses whose duration consists of only several optical cycles [1,2]. Such pulses are considerably shorter than the characteristic relaxation times in matter and are usually characterized by high-field amplitudes; and, consequently, they lead to nonlinear optical effects such as the onset of the self-induced transparency (SIT) soliton propagation regime. Both from experimental and theoretical points of view, the possibility of optical pulse reshaping and soliton formation during the passage of light waves through optical waveguides containing quantum resonant saturable absorbers is under intensive study. In fact, it has been demonstrated that soliton phenomena can be used to generate stable sub-10-fs pulses with proper choices of the peak power and minimum dispersion. It should also be noted that soliton formation due to SIT effects in a laser cavity is a strong attractor for ultrashort pulse output from mode-locked lasers [3] and, therefore, the investigation and modeling of this phenomenon is of great practical importance. In this paper we shall

focus on the planar optical waveguides with resonant nonlinearities since they are basic components of the contemporary integrated optoelectronics, and represent interest in view of future potential device applications such as ultrashort pulse generation, modulation, and switching.

On the other hand, experimental studies of the ultrafast laser dynamics in vertical-cavity surface-emitting lasers using femtosecond optical pulse excitations [4,5] undoubtedly show that new physical effects become important in this regime [6]. Therefore, it is increasingly important that methods of theoretical analysis of the generation and propagation of ultrashort optical pulses are rendered adequate to meet the needs of this rapid progression of ultrafast experimental techniques. When the laser-pulse temporal width becomes comparable to the optical period, a transition to a qualitatively new regime of strong laser-field-matter interactions is induced in which the electric field itself rather than intensity envelope drives the interaction. A number of theoretical works have demonstrated the limitations of the standard slowly varying envelope approximation (SVEA) and new phenomena have been predicted on the basis of the exact nonperturbative approach (see, e.g., Ref. [7], and references therein). Therefore, many theoretical results, obtained by using SVEA and the rate equation approximation, need to be tested carefully without invoking any of the standard approximations. In order to do that, a new fully nonperturbative model based on the Maxwell's curl-Bloch equations needs to be developed. In this respect, full-wave vector numerical

---

\*Present address: Department of Electrical and Computer Engineering, University of Arizona, Tucson, Arizona 85721.

techniques such as the finite-difference time-domain (FDTD) method have proven to be particularly useful and powerful tools for directly solving the Maxwell-Bloch system in time domain [7–9]. The main reasons for choosing the FDTD computational method in our simulations of ultrashort optical pulse propagation are:

(i) Since we shall be interested in the time evolution of the optical fields and the population dynamics of the quantum system, it is natural to carry out the modeling directly in the time domain.

(ii) FDTD is an accurate numerical technique that equally well accounts both for the guided and radiation (scattering) modes. This turns out to be of great significance for an accurate modeling of the demonstrated self-induced transparency effects, pulse reshaping, and for the validations performed against the pulse area theorem.

(iii) FDTD is a flexible method that generates a full-wave-vector solution of Maxwell's equations coupled to the first-principles quantum-mechanics model of the resonant nonlinear system (and has been done in one-dimension (1D) for a two-level system [9]).

The motivation of the present work is to develop an *ab initio* accurate and rigorous theoretical model of the spatiotemporal dynamics for ultrashort pulse propagation in two-dimensional planar optical waveguides containing resonant nonlinearities. In the most general case, this model should account for the medium polarization in two mutually orthogonal directions, and at the same time should not impose any restrictions or approximations on the electromagnetic wave propagation that would result in a limited range of validity. Within the semiclassical approach, the latter requires the solution of the full-vector Maxwell's equations in 2D. In what follows, we shall be interested in one-photon absorption processes rather than two-photon absorption, i.e., single-pulse excitations. In order to model the interaction of an ultrashort laser pulse with the medium in two spatial dimensions, we show that the minimum requirement for one-photon excitation is to consider a degenerate three-level ensemble of atoms in which two of the allowed electric-dipole transitions are excited by each of the two components of the  $E$  field in the waveguide plane. Attenuation caused by damping of the resonant dipoles or by background scattering losses is accounted for within the model by introducing phenomenological relaxation times (experimentally obtainable). In this study, we have considered the most general case of a damped ensemble of dipole oscillators chosen as representative of a homogeneously broadened degenerate three-level quantum-mechanical system of polarized atoms, which is at or near resonance with the pulse of 2D-wave radiation. Our analysis is applied to this simplified physical model for the resonant nonlinear medium. Justification for this is the well-known homogeneously broadened two-level atomic system coupled to the Maxwell's equations in 1D, which has been shown to describe successfully linear and nonlinear absorption/gain saturation effects [9,10]. The model potentially could be extended further to describe the heavy-hole (hh) exciton transition in a quantum well at the center of the Brillouin zone within the two-band formulation for the semiconductors [11–13]. Because of the spin degeneracy, the hh-

to-conduction band transition actually consists of two degenerate transitions: one for each spin state.

In order to achieve this goal, we employ the formalism developed by Hioe and Eberly [14–16] for resonant, coherent interactions of the electromagnetic wave with a multi-level quantum system within the real-vector representation. In what follows, we shall be interested in two main aspects of the physical effects, which can be described and explained satisfactorily by resonant, coherent interactions: the coherent dynamical evolution of a quantum system and the lossless propagation of electromagnetic fields through a multi level quantum system.

In particular, the description of resonant, coherent interactions of an electromagnetic wave with an  $N$ -level atomic system within the framework of the real-vector representation has attracted significant attention since the appearance of the pioneering paper by Feynman and co-workers [17]. It has been shown that when coherent processes are involved in a two-level system, it is sufficient to consider a real three-vector rather than the complex probability amplitudes in the Schrödinger equation. The equation of motion of the latter is in the form of a precession of a classical gyromagnet in a constant magnetic field. This in turn provides an elegant geometrical framework for discussing the system dynamics in terms of rotations of a real state vector in Hilbert space. Moreover, since this representation is based on the underlying complex density-matrix formalism, it allows treatment with ease of both pure and mixed quantum states, in contrast to the wave-function treatment. This formal analogy has been extended further for a spin- $J$  system in constant magnetic field for the description of a laser excitation of an  $N = 2J + 1$  level system [18]. However, the simple form of the basic equation of motion for the real vector (torque or Bloch spin equation) remains valid only for equally spaced energy levels. Preserving this simple form of the vector equation has a number of advantages. It accounts for the intrinsic symmetry of the underlying Hilbert space of the system and, therefore, is an exact description, independent of the strength, number, or time dependence of the external forces acting on the system. In addition, similar to the two-level system, the dynamical evolution can be characterized as a rotation in the real physical space of a real coherence vector. Solution of this problem has been given by Elgin [19] for a three-level system, as an extension of the two-level system, by invoking the invariance of the state vector under rotations of the  $SU(3)$  transformation group. A general solution of this problem for an  $N$ -level quantum system with arbitrary level spacing has been found by Hioe and Eberly [14]. They expanded the system Hamiltonian in the transition-projection operators that are the generators of the unitary group  $U(N)$ , where  $N$  is the number of eigenstates of the Hamiltonian. Defining further another set of operators based on the projection operators that generate the  $SU(N)$  algebra, they derived the pseudospin equation showing the time development of the coherence vector as a generalized rotation in  $N^2 - 1$  space. Special attention has been paid to the case of a three-level system [15,16,20] that represents particular interest since it provides a useful framework for studying, for example, such phenomena as two-photon resonance, three-level echoes,

population trapping, and three-level super-radiance. As a direct consequence of the general  $N$ -level case, the dynamical evolution of a three-level system can be expressed in terms of an eight-dimensional real coherence vector, thus exploiting the group-theoretical and Gell-Mann's  $SU(3)$  dynamical-symmetry properties [21].

In this paper we apply and develop further the real-vector representation formalism to the problem of single electromagnetic wave propagation and its resonant coherent interaction with a degenerate three-level quantum system in two spatial dimensions in planar optical waveguide geometry. The aim is to construct a coupled set of semiclassical Maxwell-Bloch equations in 2D, which would represent a realistic model for studying the time evolution of the optical fields during the interaction with a multilevel quantum system and the related population dynamics. The main physical result of the model is the demonstration of self-induced transparency effects in multidimensional systems. As we shall show below, the SIT-soliton behavior in 2D systems is demonstrated not only for the TEM mode, but most importantly for the  $TM_1$  mode, when the optical field couples all the three levels of the quantum system. The latter cannot be considered as a simple consequence of the reduction of the three-level system to a two-level one, since in this case the three-level system is irreducible. Moreover, we show how to modify properly the pulse area theorem to provide a criterion for reaching the SIT regime in the multidimensional case.

The outline of the paper is as follows. Section II consists of three subsections. In Sec. II A we give a brief overview of the basic equations used thereafter for the derivation of the desired pseudospin equations in 2D. The coupled set of Maxwell-Bloch equations in 2D are derived for both TM and TE waves in Secs. II B and II C, respectively. In Sec. III we describe the discretization scheme that was applied to these systems of continuum equations and provide details on the numerical methods used to solve their discrete forms. The main results of the numerical simulations are given in Sec. IV. The advantages of the present approach are summarized in Sec. V.

## II. DERIVATION OF THE MAXWELL-BLOCH EQUATIONS IN 2D

We are interested in the following guided modes of the parallel-mirror waveguide under consideration, namely, the plane-polarized TEM mode  $\mathbf{E}=(0,E_y,0)$  and  $\mathbf{H}=(H_x,0,0)$  (which is also referred to as the  $TM_0$  mode according to its classification in electromagnetic theory), the TM mode  $\mathbf{H}=(H_x,0,0)$  and  $\mathbf{E}=(0,E_y,E_z)$  [Fig. 1(a)], specifically the first-order  $TM_1$  mode; and the TE mode  $\mathbf{E}=(E_x,0,0)$  and  $\mathbf{H}=(0,H_y,H_z)$  [Fig. 1(b)].

### A. Pseudospin equations for an $N$ -level system

The dynamical evolution of an  $N$ -level atomic system is governed by the equation of motion for the density matrix  $\hat{\rho}$  (Liouville equation):

$$i\hbar \frac{\partial \hat{\rho}}{\partial t} = [\hat{H}, \hat{\rho}]. \quad (1)$$

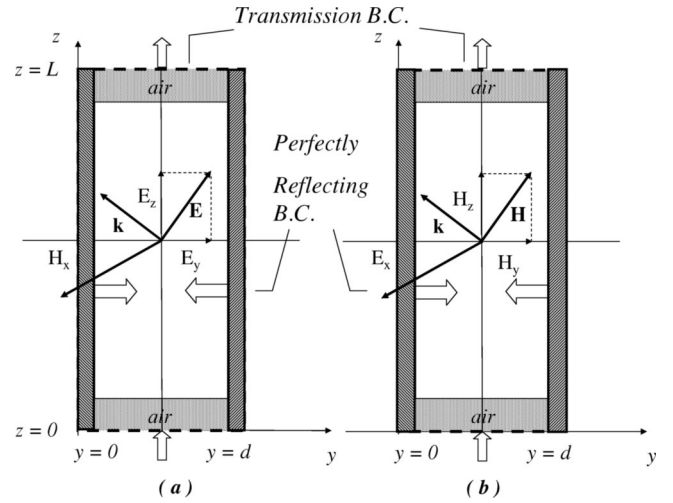


FIG. 1. Simulation domain geometry and electromagnetic field configuration of the (a) TM and (b) TE guided modes in the parallel-plate mirror optical waveguide. The boundary conditions are indicated by arrows at the respective interfaces [upward pointing arrows and dashed lines indicate transmission boundaries; left and right arrows (shaded areas that have to be considered as infinitesimally thin) indicate perfectly reflecting boundaries].

Exploiting the symmetry of the rotations under the  $SU(N)$  group, it has been shown [14–16,19] that the density matrix  $\rho(t)$  and the system Hamiltonian  $H(t)$  can be expressed in terms of the  $N^2 - 1$  generators  $\lambda_j$  of the  $SU(N)$  Lie algebra according to

$$\hat{\rho}(t) = \frac{1}{N} \hat{I} + \frac{1}{2} \sum_{j=1}^{N^2-1} S_j(t) \hat{\lambda}_j \quad (2)$$

and

$$\hat{H}(t) = \frac{1}{2} \hbar \left( \frac{2}{N} \left[ \sum_{k=1}^N \omega_k \right] \hat{I} + \sum_{j=1}^{N^2-1} \gamma_j(t) \hat{\lambda}_j \right), \quad (3)$$

where  $\hbar \omega_k$  is the energy of the level  $k$  and  $\hat{I}$  is the identity operator. Assuming that the Gell-Mann generators  $\{\lambda_j, j=1,2,\dots,N\}$  are chosen to satisfy the orthogonality relations for any  $N$ ,

$$\text{Tr}(\hat{\lambda}_j \hat{\lambda}_k) = 2 \delta_{jk}, \quad (4)$$

the coefficients  $S_j(t)$  and  $\gamma_j(t)$  are given by

$$S_j(t) = \text{Tr}[\hat{\rho}(t) \hat{\lambda}_j], \quad (5a)$$

$$\hbar \gamma_j(t) = \text{Tr}[\hat{H}(t) \hat{\lambda}_j]. \quad (5b)$$

The time evolution of the density matrix can be expressed in terms of the evolution of an  $(N^2 - 1)$ -dimensional real state vector  $\mathbf{S}=(S_1, S_2, \dots, S_{N^2-1})$ , called the pseudospin or coherence vector, in the Hilbert space that is described by the pseudospin equation

TABLE I. Nonvanishing components of the antisymmetric tensor of the structure constants  $f_{ijk}$ .

$ijk$	147	135	126	432	465	736	752	368	258
$f_{ijk}$	1	-1/2	-1/2	-1/2	-1/2	1/2	1/2	$\frac{\sqrt{3}}{2}$	$\frac{\sqrt{3}}{2}$

$$\dot{S}_j(t) = \sum_{k=1}^{N^2-1} \Lambda_{jk}(t) S_k(t), \quad j=1,2,\dots,N^2-1, \quad (6)$$

where the dot stands for the time derivative and

$$\Lambda_{jk} = -\frac{1}{2i\hbar} \text{Tr}(\hat{H}[\hat{\lambda}_j, \hat{\lambda}_k]). \quad (7)$$

Equation (6) represents a generalization of the torque equation (or real three-vector equation) obtained for a two-level system [17].

Let us consider now a three-level atomic system. A possible choice of the Gell-Mann SU(3) generators satisfying Eq. (4) is given by

$$\begin{aligned} \lambda_1 &= \begin{pmatrix} 0 & 1 & 0 \\ 1 & 0 & 0 \\ 0 & 0 & 0 \end{pmatrix}, & \lambda_2 &= \begin{pmatrix} 0 & 0 & 0 \\ 0 & 0 & 1 \\ 0 & 1 & 0 \end{pmatrix}, \\ \lambda_3 &= \begin{pmatrix} 0 & 0 & 1 \\ 0 & 0 & 0 \\ 1 & 0 & 0 \end{pmatrix}, & \lambda_4 &= \begin{pmatrix} 0 & i & 0 \\ -i & 0 & 0 \\ 0 & 0 & 0 \end{pmatrix}, \\ \lambda_5 &= \begin{pmatrix} 0 & 0 & 0 \\ 0 & 0 & i \\ 0 & -i & 0 \end{pmatrix}, & \lambda_6 &= \begin{pmatrix} 0 & 0 & i \\ 0 & 0 & 0 \\ -i & 0 & 0 \end{pmatrix}, \\ \lambda_7 &= \begin{pmatrix} -1 & 0 & 0 \\ 0 & 1 & 0 \\ 0 & 0 & 0 \end{pmatrix}, & \lambda_8 &= \frac{1}{\sqrt{3}} \begin{pmatrix} -1 & 0 & 0 \\ 0 & -1 & 0 \\ 0 & 0 & 2 \end{pmatrix}. \end{aligned}$$

After transformation to a rotating wave coordinate frame, the equation of motion (6) takes the form

$$\dot{S}_i = f_{ijk} \gamma_j S_k; \quad i, j, k=1,\dots,8, \quad (8)$$

where summation over  $j, k$  is assumed,  $\gamma_j$  are the components of the torque vector and  $f_{ijk}$  is a fully antisymmetric tensor of the structure constants of the SU(3) group that for  $N=2$  is simply the fully antisymmetric, unit tensor  $\varepsilon_{ijk}$ . The only nonvanishing values of  $f_{ijk}$  are the permutations given in Table I.

Finally, the system Hamiltonian in the presence of a dipole coupling perturbation can be written in the form

$$\hat{H}(t) = \hat{H}_0 + \hat{H}_{\text{int}}(t) = \hat{H}_0 + e\mathbf{E} \cdot \hat{\mathbf{Q}}, \quad (9)$$

where  $\hat{H}_0$  is the unperturbed Hamiltonian (in the absence of an electromagnetic wave) and  $\hat{\mathbf{Q}}$  is the local displacement operator whose expectation value gives the local displacement vector  $\mathbf{q}$ .

### B. Maxwell-Bloch equations for transverse magnetic waves

Maxwell's equations in an isotropic medium read

$$\begin{aligned} \frac{\partial \mathbf{H}}{\partial t} &= -\frac{1}{\mu} \nabla \times \mathbf{E}, \\ \frac{\partial \mathbf{E}}{\partial t} &= \frac{1}{\varepsilon} \nabla \times \mathbf{H} - \frac{1}{\varepsilon} \frac{\partial \mathbf{P}}{\partial t}, \end{aligned} \quad (10)$$

where  $\varepsilon$  and  $\mu$  are given functions of space and the polarization current  $\mathbf{J} = \partial \mathbf{P} / \partial t$ . For a TM wave  $\mathbf{H} = (H_x, 0, 0)$  and  $\mathbf{E} = (0, E_y, E_z)$ , we find in the 2D case,

$$\begin{aligned} \frac{\partial H_x}{\partial t} &= -\frac{1}{\mu} \frac{\partial E_z}{\partial y} + \frac{1}{\mu} \frac{\partial E_y}{\partial z}, \\ \frac{\partial E_y}{\partial t} &= \frac{1}{\varepsilon} \frac{\partial H_x}{\partial z} - \frac{1}{\varepsilon} \frac{\partial P_y}{\partial t}, \\ \frac{\partial E_z}{\partial t} &= -\frac{1}{\varepsilon} \frac{\partial H_x}{\partial y} - \frac{1}{\varepsilon} \frac{\partial P_z}{\partial t}. \end{aligned} \quad (11)$$

In the case of a TM wave, in-plane polarization of the medium is induced along the propagation axis  $z$  and in a transverse direction [Fig. 1(a)]. In order to derive the Maxwell-Bloch equations in 2D, we shall consider a degenerate three-level atomic system in which two electric dipole transitions are allowed to be excited by a linearly polarized monochromatic electromagnetic wave with frequency equal (or close) to the atomic resonance frequency (Fig. 2). Let us assume that the energy 0 is chosen at the ground-state energy  $E_1 = 0$ , and the energy corresponding to the excited levels is  $\hbar\omega_0$ . The unperturbed Hamiltonian of a degenerate three-level system can then be written in the following simple form:

$$\hat{H}_0 = \begin{pmatrix} 0 & 0 & 0 \\ 0 & \hbar\omega_0 & 0 \\ 0 & 0 & \hbar\omega_0 \end{pmatrix}. \quad (12)$$

If the polarization density  $\mathbf{P}$  is along a general direction in the plane ( $y, z$ ), the local displacement vector  $\mathbf{q}$  can be represented by its components along the  $y$  and  $z$  axes, and the displacement operator in turn can be decoupled into two operators, according to

$$\hat{\mathbf{Q}} = q_0 \left\{ \begin{pmatrix} 0 & 1 & 0 \\ 1 & 0 & 0 \\ 0 & 0 & 0 \end{pmatrix} \mathbf{e}_y + \begin{pmatrix} 0 & 0 & 1 \\ 0 & 0 & 0 \\ 1 & 0 & 0 \end{pmatrix} \mathbf{e}_z \right\}, \quad (13)$$

where  $q_0$  is the typical atomic length scale, and  $\mathbf{e}_y, \mathbf{e}_z$  are the unit vectors along the  $y$  and  $z$  axes. In any physical medium,

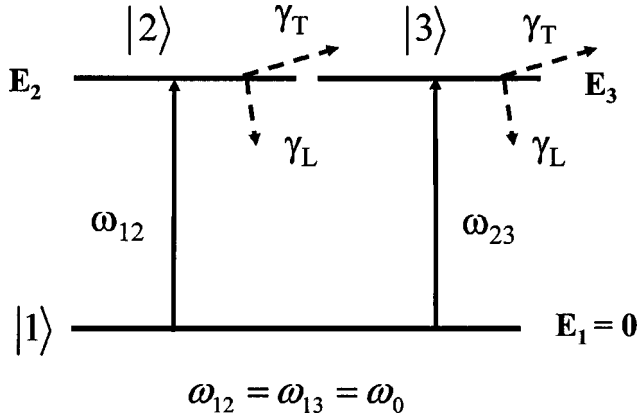


FIG. 2. Energy-level diagram of a three-level quantum system with a doubly degenerate excited state (with, e.g., spin degeneracy, level  $|2\rangle$  represents spin-down state and level  $|3\rangle$  is the spin-up state) at resonance. Two electric dipole transitions can be excited by the monochromatic electromagnetic wave. The level difference angular frequencies are  $\omega_{12} = (E_2 - E_1)/\hbar$ ,  $\omega_{13} = (E_3 - E_1)/\hbar$ , and  $\omega_{12} = \omega_{13} = \omega_0$ . The energy zero is chosen at the ground-state energy  $E_1 = 0$ .  $\gamma_L$  accounts for the decay of the population from the upper levels to the ground level;  $\gamma_T$  represents the dephasing rate (transverse relaxation rate).

$q_0$  represents a measure of the separation of the charges in the dipole and is given by a specific computation of the size of the electron orbit, e.g., the Bohr radius of hydrogen atom. For simplicity, in the calculations we shall assume  $q_0$  to be of the order of magnitude of  $\sim 1 \text{ \AA}$ . As a result, the dipole coupling interaction Hamiltonian can be written as

$$\hat{H}_{\text{int}}(t) = \hbar \begin{pmatrix} 0 & \Omega_y & \Omega_z \\ \Omega_y & 0 & 0 \\ \Omega_z & 0 & 0 \end{pmatrix}, \quad (14)$$

where we have defined Rabi frequencies of the oscillations along  $y$  and  $z$  according to

$$\Omega_y = \frac{\wp}{\hbar} E_y, \quad \Omega_z = \frac{\wp}{\hbar} E_z, \quad (15)$$

and  $\wp = eq_0$  is the dipole coupling constant. Therefore, the total Hamiltonian acquires the form

$$\hat{H}(t) = \hbar \begin{pmatrix} 0 & \Omega_y & \Omega_z \\ \Omega_y & \omega_0 & 0 \\ \Omega_z & 0 & \omega_0 \end{pmatrix}. \quad (16)$$

Now we can easily calculate the components of the torque vector from Eq. (5b); this leads to the following time-independent torque vector:

$$\boldsymbol{\gamma} = \left( 2\Omega_y, 0, 2\Omega_z, 0, 0, 0, \omega_0, \frac{\omega_0}{\sqrt{3}} \right). \quad (17)$$

Taking into account only the nonvanishing structure constants (see Table I), using the antisymmetry relations between the possible permutations of indices, and performing the summation over  $j$  and  $k$  in Eq. (8), we obtain finally the following set of equations for the components of the coherence vector:

$$\frac{\partial S_1}{\partial t} = -\omega_0 S_4 - \Omega_z S_5,$$

$$\frac{\partial S_2}{\partial t} = \Omega_z S_4 + \Omega_y S_6,$$

$$\frac{\partial S_3}{\partial t} = \Omega_y S_5 - \omega_0 S_6,$$

$$\frac{\partial S_4}{\partial t} = \omega_0 S_1 - \Omega_z S_2 - 2\Omega_y S_7,$$

$$\frac{\partial S_5}{\partial t} = \Omega_z S_1 - \Omega_y S_3, \quad (18)$$

$$\frac{\partial S_6}{\partial t} = -\Omega_y S_2 + \omega_0 S_3 - \Omega_z S_7 - \sqrt{3}\Omega_z S_8,$$

$$\frac{\partial S_7}{\partial t} = 2\Omega_y S_4 + \Omega_z S_6,$$

$$\frac{\partial S_8}{\partial t} = \sqrt{3}\Omega_z S_6.$$

These equations can be written in a more compact matrix form as

$$\frac{\partial}{\partial t} \begin{pmatrix} S_1 \\ S_2 \\ S_3 \\ S_4 \\ S_5 \\ S_6 \\ S_7 \\ S_8 \end{pmatrix} = \begin{pmatrix} 0 & 0 & 0 & -\omega_0 & -\Omega_z & 0 & 0 & 0 \\ 0 & 0 & 0 & \Omega_z & 0 & \Omega_y & 0 & 0 \\ 0 & 0 & 0 & 0 & \Omega_y & -\omega_0 & 0 & 0 \\ \omega_0 & -\Omega_z & 0 & 0 & 0 & 0 & -2\Omega_y & 0 \\ \Omega_z & 0 & -\Omega_y & 0 & 0 & 0 & 0 & 0 \\ 0 & -\Omega_y & \omega_0 & 0 & 0 & 0 & -\Omega_z & -\sqrt{3}\Omega_z \\ 0 & 0 & 0 & 2\Omega_y & 0 & \Omega_z & 0 & 0 \\ 0 & 0 & 0 & 0 & 0 & \sqrt{3}\Omega_z & 0 & 0 \end{pmatrix} \begin{pmatrix} S_1 \\ S_2 \\ S_3 \\ S_4 \\ S_5 \\ S_6 \\ S_7 \\ S_8 \end{pmatrix}, \quad (19)$$

and hence as

$$\frac{\partial \mathbf{S}}{\partial t} = \mathcal{M}^{\text{TM}} \mathbf{S},$$

where the matrix  $\mathcal{M}^{\text{TM}}$  is an  $8 \times 8$  antisymmetric matrix with only nine independent components.

In order to couple the semiclassical Maxwell's equations with the quantum-mechanical pseudospin equations, we need to find a relationship between the polarization and the components of the coherence vector. The macroscopic polarization of the medium is given by the expectation value of the dipole moment operator:

$$\mathbf{P} = -N_a e \langle \hat{\mathbf{Q}} \rangle = -N_a e \text{Tr}(\hat{\rho} \hat{\mathbf{Q}}), \quad (20)$$

where  $N_a$  is the density of the polarizable atoms in the medium. Using Eq. (2), we can calculate the polarization components along  $y$  and  $z$  from Eq. (20), taking into account the explicit form of the displacement operator (13), to obtain the following relationships:

$$P_y = -\varphi N_a S_1, \quad (21)$$

$$P_z = -\varphi N_a S_3. \quad (22)$$

We can easily extend the above formalism for a three-level system in the presence of relaxation effects by introducing phenomenological nonuniform decay times  $T_1, \dots, T_8$  that govern the relaxation of the pseudospin vector components to their equilibrium values. The coherence vector will then satisfy the equation

$$\frac{\partial \mathbf{S}}{\partial t} = \mathcal{M}^{\text{TM}} \mathbf{S} - \sigma (\mathbf{S} - \mathbf{S}_E), \quad (23)$$

where  $\mathbf{S}_E$  is the equilibrium value to which  $\mathbf{S}$  tends to in the absence of any driving field, and

$$\sigma = \text{diag}(1/T_1, 1/T_2, \dots, 1/T_8) \quad (24)$$

is the diagonal matrix of the nonuniform relaxation rates. Note that, as has been pointed out in Ref. [20], the equilibrium (or zero-field) coherence vector  $\mathbf{S}_E$  is determined by incoherent sources as a thermal reservoir or external pumping that maintains the system at a definite level of excitation. Dephasing causes the first six components of  $\mathbf{S}_E$  to vanish, and only the population terms ( $S_7$  and  $S_8$ ) depend on the initial occupation of the levels.

Equations (11) and (21)–(24) form a set of 13 coupled equations for the 13 unknowns:  $H_x, E_y, E_z, P_y, P_z, S_1, \dots, S_8$ , and hence its solution is fully determined.

### C. Maxwell-Bloch equations for transverse electric waves

In the case of a TE wave, we follow the same formalism. Maxwell's equations in 2D for the TE wave  $\mathbf{E} = (E_x, 0, 0)$ ,  $\mathbf{H} = (0, H_y, H_z)$  read

$$\begin{aligned} \frac{\partial H_y}{\partial t} &= -\frac{1}{\mu} \frac{\partial E_x}{\partial z}, \\ \frac{\partial H_z}{\partial t} &= \frac{1}{\mu} \frac{\partial E_x}{\partial y}, \end{aligned} \quad (25)$$

$$\frac{\partial E_x}{\partial t} = \frac{1}{\varepsilon} \left( \frac{\partial H_z}{\partial y} - \frac{\partial H_y}{\partial z} \right) - \frac{1}{\varepsilon} \frac{\partial P_x}{\partial t}.$$

Since for TE waves the polarization exists only along the  $x$  axis, the local displacement vector  $\mathbf{q}$  is parallel to the electric field, and the displacement operator is of the form

$$\hat{\mathbf{Q}} = q_0 \begin{pmatrix} 0 & 1 & 0 \\ 1 & 0 & 0 \\ 0 & 0 & 0 \end{pmatrix} \mathbf{e}_x, \quad (26)$$

where  $\mathbf{e}_x$  is a unit vector along the  $x$  axis. Therefore the interaction Hamiltonian takes the form

$$\hat{H}(t) = \begin{pmatrix} 0 & \Omega_x & 0 \\ \Omega_x & \omega_0 & 0 \\ 0 & 0 & \omega_0 \end{pmatrix}, \quad (27)$$

where we have defined a Rabi frequency along the  $x$  axis, according to

$$\Omega_x = \frac{\varphi}{\hbar} E_x. \quad (28)$$

Analogous to the TM case, we calculate the components of the time-independent torque vector  $\gamma = [2\Omega_x, 0, 0, 0, 0, \omega_0, (\omega_0/\sqrt{3})]$  and substitute them in the pseudospin equations (8), taking into account the asymmetric property of the structure constant tensor to determine the nonvanishing permutations of the indices (see Table I). This gives the following set of equations for the components of the coherence vector:

$$\begin{aligned} \frac{\partial S_1}{\partial t} &= -\omega_0 S_4, & \frac{\partial S_2}{\partial t} &= \Omega_x S_6, \\ \frac{\partial S_3}{\partial t} &= \Omega_x S_5 - \omega_0 S_6, & \frac{\partial S_4}{\partial t} &= \omega_0 S_1 - 2\Omega_x S_7, \\ \frac{\partial S_5}{\partial t} &= -\Omega_x S_3, & \frac{\partial S_6}{\partial t} &= -\Omega_x S_2 + \omega_0 S_3, \\ \frac{\partial S_7}{\partial t} &= 2\Omega_x S_4, & \frac{\partial S_8}{\partial t} &= 0, \end{aligned} \quad (29)$$

or equivalently in the matrix form

$$\frac{\partial}{\partial t} \begin{pmatrix} S_1 \\ S_2 \\ S_3 \\ S_4 \\ S_5 \\ S_6 \\ S_7 \end{pmatrix} = \begin{pmatrix} 0 & 0 & 0 & -\omega_0 & 0 & 0 & 0 \\ 0 & 0 & 0 & 0 & 0 & \Omega_x & 0 \\ 0 & 0 & 0 & 0 & \Omega_x & -\omega_0 & 0 \\ \omega_0 & 0 & 0 & 0 & 0 & 0 & -2\Omega_x \\ 0 & 0 & -\Omega_x & 0 & 0 & 0 & 0 \\ 0 & -\Omega_x & \omega_0 & 0 & 0 & 0 & 0 \\ 0 & 0 & 0 & 2\Omega_x & 0 & 0 & 0 \end{pmatrix} \begin{pmatrix} S_1 \\ S_2 \\ S_3 \\ S_4 \\ S_5 \\ S_6 \\ S_7 \end{pmatrix}. \quad (30)$$

The resulting set of nonuniformly damped equations is correspondingly

$$\frac{\partial \mathbf{S}}{\partial t} = \mathcal{M}^{\text{TE}} \mathbf{S} - \sigma (\mathbf{S} - \mathbf{S}_E), \quad (31)$$

where  $\sigma$  is given by Eq. (24).

Again we need to determine whatever additional equations relate the macroscopic polarization in Maxwell's equations to the components of the coherence vector. These can be obtained from Eqs. (2), (20), and (26). One simply finds that

$$P_x = -\varphi N_a S_1. \quad (32)$$

As should be expected from the two-level system results (see Eq. (10), Ref. [9]), the polarization along the electric field depends on the corresponding component of the coherence vector.

Equations (25), (31), and (32) form a set of 12 equations for the 12 unknowns  $E_x, H_y, H_z, P_x, S_1, \dots, S_8$  and, therefore, its solution is fully determined.

It can be easily proven that the TE case is equivalent to a two-level system case. Let us set  $S_1 = \rho_1, S_4 = -\rho_2, S_7 = \rho_3$ , where  $\rho_i, i = 1, 2, 3$  is the real three-vector representation of the density matrix [17]. Then from the first, fourth, and the seventh equations of the set (29), one obtains the following system:

$$\begin{aligned} \frac{\partial \rho_1}{\partial t} &= \omega_0 \rho_2, \\ \frac{\partial \rho_2}{\partial t} &= -\omega_0 \rho_1 + 2\Omega_x \rho_3, \\ \frac{\partial \rho_3}{\partial t} &= -2\Omega_x \rho_2. \end{aligned} \quad (33)$$

This system coincides with the undamped set of two-level equations from Ref. [9]. The rest of the equations for  $S_2, S_3, S_5, S_6$  are decoupled from this system. This decoupling can be understood in terms of the elements of the density matrix. In particular, the coherence vector components are related to the elements of the density matrix by the following relations:

$$S_1 = \hat{\rho}_{12} + \hat{\rho}_{21}, \quad S_2 = \hat{\rho}_{23} + \hat{\rho}_{32},$$

$$S_3 = \hat{\rho}_{13} + \hat{\rho}_{31}, \quad S_4 = -i(\hat{\rho}_{12} - \hat{\rho}_{21}),$$

$$S_5 = -i(\hat{\rho}_{23} - \hat{\rho}_{32}), \quad S_6 = -i(\hat{\rho}_{13} - \hat{\rho}_{31}),$$

$$S_7 = -(\hat{\rho}_{11} - \hat{\rho}_{22}), \quad S_8 = -\frac{1}{\sqrt{3}}(\hat{\rho}_{11} + \hat{\rho}_{22} - 2\hat{\rho}_{33}). \quad (34)$$

By inspecting the set (34), one observes that the equations for  $S_2, S_3, S_5, S_6$  do contain  $\rho$  elements with the subscript 3 corresponding to the third level. Therefore for a two-level system these components do not have physical meaning, and the whole system (29) is reduced to Eq. (33).

### III. NUMERICAL IMPLEMENTATION

We shall consider first the numerical implementation of the semiclassical Maxwell-Bloch model for the TM optical wave. For a TM wave  $\mathbf{H} = (H_x, 0, 0)$  and  $\mathbf{E} = (0, E_y, E_z)$ , the resulting damped set of equations given in Sec. II B explicitly read

$$\begin{aligned} \frac{\partial H_x}{\partial t} &= -\frac{1}{\mu} \frac{\partial E_z}{\partial y} + \frac{1}{\mu} \frac{\partial E_y}{\partial z}, \\ \frac{\partial E_y}{\partial t} &= \frac{1}{\varepsilon} \frac{\partial H_x}{\partial z} - \frac{1}{\varepsilon} \frac{\partial P_y}{\partial t}, \end{aligned} \quad (35a)$$

$$\begin{aligned} \frac{\partial E_z}{\partial t} &= -\frac{1}{\varepsilon} \frac{\partial H_x}{\partial y} - \frac{1}{\varepsilon} \frac{\partial P_z}{\partial t}, \\ P_y &= -\varphi N_a S_1, \\ P_z &= -\varphi N_a S_3; \end{aligned} \quad (35b)$$

$$\frac{\partial S_1}{\partial t} = -\omega_0 S_4 - \Omega_z S_5 - \frac{1}{T_1} S_1,$$

$$\frac{\partial S_2}{\partial t} = \Omega_z S_4 + \Omega_y S_6 - \frac{1}{T_2} S_2,$$

$$\frac{\partial S_3}{\partial t} = \Omega_y S_5 - \omega_0 S_6 - \frac{1}{T_3} S_3,$$

$$\frac{\partial S_4}{\partial t} = \omega_0 S_1 - \Omega_z S_2 - 2\Omega_y S_7 - \frac{1}{T_4} S_4,$$

$$\begin{aligned}
\frac{\partial S_5}{\partial t} &= \Omega_z S_1 - \Omega_y S_3 - \frac{1}{T_5} S_5, \\
\frac{\partial S_6}{\partial t} &= -\Omega_y S_2 + \omega_0 S_3 - \Omega_z S_7 - \sqrt{3} \Omega_z S_8 - \frac{1}{T_6} S_6, \\
\frac{\partial S_7}{\partial t} &= 2\Omega_y S_4 + \Omega_z S_6 - \frac{1}{T_7} (S_7 - S_{7e}), \\
\frac{\partial S_8}{\partial t} &= \sqrt{3} \Omega_z S_6 - \frac{1}{T_8} (S_8 - S_{8e}). \tag{35c}
\end{aligned}$$

The coupling between the 2D Maxwell's equations and the equations describing the time evolution of the quantum system is performed by substituting  $P_y$  and  $P_z$  from Eq. (35b) and subsequently  $\partial S_1/\partial t$ ,  $\partial S_3/\partial t$  from Eq. (35c) into Eq. (35a), thus obtaining

$$\begin{aligned}
\frac{\partial H_x}{\partial t} &= -\frac{1}{\mu} \frac{\partial E_z}{\partial y} + \frac{1}{\mu} \frac{\partial E_y}{\partial z}, \\
\frac{\partial E_y}{\partial t} &= \frac{1}{\varepsilon} \frac{\partial H_x}{\partial z} - \frac{N_a \wp}{\varepsilon T_1} S_1 - \frac{N_a \wp \omega_0}{\varepsilon} S_4 - \frac{N_a \wp \Omega_z}{\varepsilon} S_5, \tag{35d}
\end{aligned}$$

$$\frac{\partial E_z}{\partial t} = -\frac{1}{\varepsilon} \frac{\partial H_x}{\partial y} - \frac{N_a \wp}{\varepsilon T_3} S_3 - \frac{N_a \wp \Omega_y}{\varepsilon} S_5 - \frac{N_a \wp \omega_0}{\varepsilon} S_6.$$

Equations (35c) and (35d) form a system of first-order differential equations. Equations (35c) and (35d) are discretized using finite differences on a two-dimensional Yee grid [22], where the quantum system material variables ( $S_1, \dots, S_8$ ) are assigned to the empty nodes in the grid (see the Appendix). In order to associate an electric field at the locations of the empty nodes, where the polarization components are given, or to define values of the atomic variables at half steps in accordance with the Yee algorithm, we perform averaging over the nearest neighbors of the current node as described in the Appendix. We have applied the predictor-corrector iterative scheme introduced in Ref. [9] to solve numerically the semiclassical Maxwell-pseudospin system. This approach allows the solution of all the equations in the system at each time step. It has been pointed out therein that the predictor-corrector scheme has numerous advantages with respect to other schemes. The predictor-corrector method has proved to be applicable and quite efficient in solving a great number of first-order differential equations simultaneously, as we shall show in Sec. IV.

In what follows, we shall consider the geometry of the parallel-plate mirror optical waveguide shown in Fig. 1 that is composed of a slab waveguide with bottom and top air buffers. We have applied absorbing boundary conditions at the interfaces  $z=0$  and  $L$  (see Fig. 1) based on the Engquist-Majda one-way wave equation [23] within a one-term Taylor-series approximation. The one-way wave equations have been discretized using the Mur finite-difference scheme [24], resulting in the following time-stepping algorithm for the electric-field components along the  $z=0$  grid boundary:

$$\begin{aligned}
E_z|_{0,j}^{k+1} &= -E_z|_{1,j}^{k-1} + S_1(E_z|_{1,j}^{k+1} + E_z|_{0,j}^{k-1}) + S_2(E_z|_{0,j}^k + E_z|_{1,j}^k) \\
&\quad + S_3[E_z|_{0,j+1}^k - 2E_z|_{0,j}^k + E_z|_{0,j-1}^k + E_z|_{1,j+1}^k \\
&\quad - 2E_z|_{1,j}^k + E_z|_{1,j-1}^k], \tag{36}
\end{aligned}$$

where the coefficients  $S_i^{\pm}$  ( $i=1,2,3$ ) are given by

$$\begin{aligned}
S_1^{\pm} &= \frac{c \Delta t \mp \Delta z}{c \Delta t \pm \Delta z}, \\
S_2^{\pm} &= \frac{2 \Delta z}{\pm c \Delta t + \Delta z}, \tag{37} \\
S_3^{\pm} &= \frac{(c \Delta t)^2 \Delta z}{2(\Delta y)^2 (\pm c \Delta t + \Delta z)}.
\end{aligned}$$

The constant  $c$  is the propagation speed at any spatial grid point,  $\Delta y$  and  $\Delta z$  are the spatial steps along the  $y$  and  $z$  axes, and  $\Delta t$  is the time step.

An analogous approximate analytical absorbing boundary condition can be derived for the upper grid boundary  $z=L$  (Fig. 1). The only difference between this one and the  $z=0$  boundary conditions is the sign of the propagation velocity  $c$ , thus implying different coefficients  $S_i^{\pm}$ . The boundary conditions imposed on the side walls of the waveguide ( $y=0$  and  $y=d$ ) are those appropriate for a perfectly reflecting surface, i.e.,  $E_{\tan} = E_z = 0$ .

The absorbing boundary conditions applied at the input ( $z=0$ ) and output ( $z=L$ ) facets of the structure have proven to be sufficiently accurate for the purpose of the present study. However, we are envisaging to implement more rigorous Berenger perfectly matched layer absorbing boundary conditions in the future [25]. The perfectly reflecting boundary conditions correspond to the actual geometry of a parallel-mirror waveguide; however, more realistic boundary conditions would be again absorbing (or transmitting) boundaries that would account for the evanescent field outside the real waveguide. In a more realistic case, the numerically computed guided mode of a real waveguide should be applied as a source pulse excitation.

The time evolution of a degenerate three-level quantum system in the presence of an electric field has the character of a Goursat initial-boundary problem. The latter is well posed if the initial time history of the electric field is given along some characteristic (e.g., the lower boundary  $z=0$ ). We choose the source field to be initially a plane-polarized TEM guided mode of the parallel-mirror waveguide, i.e. the  $TM_0$  mode, with amplitude  $E_0$ , carrier frequency equal to the resonant transition frequency  $\omega_0$  of the degenerate three-level system, and an arbitrary envelope. Numerical simulations have been performed with a sine pulse with a carrier frequency set at the resonance value  $\omega = \omega_0$  and modulated by a hyperbolic-secant envelope, and a Gaussian envelope as the test pulse shape, namely,

$$E_y(z=0, y, t) = \begin{cases} E_0 \operatorname{sech}(10\Gamma) \sin(\omega_0 t) \\ E_0 \exp\left(\left(\frac{t-t_0}{t_{\text{decay}}}\right)^2\right) \sin(\omega_0 t), \end{cases} \quad (38)$$

$$E_z(z=0, y, t) = 0,$$

where  $T_p$  is the pulse duration and the constant  $\Gamma = [t - (T_p/2)] / (T_p/2)$ . The Gaussian pulse is centered at the time moment  $t_0 = k_0 \Delta t$ , where  $k_0$  is the integer time step, and has a  $1/e$  characteristic decay of  $k_{\text{decay}}$  time steps ( $t_{\text{decay}} = k_{\text{decay}} \Delta t$ ). If a smooth transition from zero to the Gaussian pulse is required,  $k_0$  should be taken at least as  $3k_{\text{decay}}$  (Ref. [25]).

For investigation of the more general TM case, we apply as a source the fundamental  $\text{TM}_1$  guided mode of the parallel-mirror light waveguide (see, e.g., Ref. [26]) and a hyperbolic-secant (HS) modulated sine wave whose carrier frequency is set to the atomic resonance value:

$$E_y(z=0, y, t) = E_0 c_1 \cos\left(\frac{\pi y}{d}\right) \operatorname{sech}(10\Gamma) \sin(\omega_0 t),$$

$$E_z(z=0, y, t) = -E_0 c_2 \sin\left(\frac{\pi y}{d}\right) \operatorname{sech}(10\Gamma) \cos(\omega_0 t), \quad (39)$$

$$c_1 = \frac{\left[\frac{\omega_0^2 n^2}{c_0^2} - \left(\frac{\pi}{d}\right)^2\right]^{1/2}}{\omega_0 \varepsilon_0 n^2}; \quad c_2 = \frac{\pi}{\omega_0 \varepsilon_0 n^2 d},$$

where  $d$  is the separation between the mirrors and  $n$  is the refractive index of the medium between the mirrors.

In order to ensure numerical stability, the time step is chosen according to the two-dimensional Courant condition:

$$\Delta t \leq \frac{1}{c \left[ \frac{1}{(\Delta y)^2} + \frac{1}{(\Delta z)^2} \right]^{1/2}}. \quad (40)$$

In all of the simulations we assumed that the degenerate three-level system was at resonance and the carrier frequency was taken to be equal to the transition frequency, i.e.,  $\omega = \omega_0 = 2\pi f_0$ , where  $f_0 = 2.0 \times 10^{14} \text{ s}^{-1}$ , corresponding to the wavelength  $\lambda = 1.5 \mu\text{m}$ . In all of the simulations, the pulse duration was set to  $T_p = 100 \text{ fs}$ . With a value of  $q_0 \sim 1 \text{ \AA}$ , the coupling coefficient equals  $\wp = 1.0 \times 10^{-29} \text{ C m}$ . The number of dipoles per unit volume was set equal to  $N_{\text{dipoles}} = 10^{24} \text{ m}^{-3}$ . The relaxation times corresponding to the decay of the real state vector components were set to the uniform value  $T_1 = \dots = T_8 = 1.0 \times 10^{-10} \text{ s}$  in order to satisfy the SIT criterion, namely  $T_1, T_2, \dots, T_8 \gg T_p$ . Moreover, uniform relaxation times avoid any pulse distortions that could arise eventually if asymmetries in the relaxation times were imposed.

## IV. SIMULATION RESULTS AND DISCUSSION

### A. $\text{TM}_0$ guided mode SIT soliton

We have performed a number of validation studies to investigate numerically the formation of a SIT quasisoliton in two spatial dimensions within the parallel-plate mirror optical waveguide filled with an active medium consisting of degenerate three-level quantum absorbers. Both the  $\text{TM}_0$  and the  $\text{TM}_1$  excitation mode cases were considered. The numerical results indicate the realization of SIT solitons in both of these multidimensional systems.

Let us consider first the simpler  $\text{TM}_0$  (TEM-wave) case. The source pulse is a plane wave polarized along the transverse direction perpendicular to the plane of the waveguide (Fig. 1). It is excited with a hyperbolic-secant modulated sine wave at the atomic resonance frequency [see the upper line of Eq. (38)].

It can be shown easily that this case is equivalent to the propagation of a one-dimensional plane wave through a resonant two-level medium [9] by considering a cross section (slice) of the field distribution along the propagation axis perpendicular to the plane. Therefore, we expected that the pulse area theorem [27,28] should still be applicable along the propagation direction and performed several tests to verify its predictions for the maximum field amplitude and pulse duration. The pulse area at a given time is given by

$$\theta(z, t) = \frac{\wp}{\hbar} \int_{-\infty}^t A(z, t') dt', \quad (41)$$

where

$$A(z, t) = E_0 \operatorname{sech}\left[\frac{t - \frac{z}{V}}{\tau}\right] = E_0 \operatorname{sech}(10\Gamma)$$

is the electric-field envelope,  $V$  is the pulse (group) velocity in the medium, and  $\tau = (T_p/20)$ ,  $T_p$  being the pulse duration. The area of the entire pulse is

$$\theta_{\text{pulse}}(z) = \frac{\wp}{\hbar} \int_{-\infty}^{\infty} A(z, t') dt'. \quad (42)$$

Let us consider pulse propagation in an absorbing medium. In particular, pulses with areas less than  $\pi$  should be completely absorbed within several absorption lengths in the active medium according to the pulse area theorem in accordance with the usual Beer's law of absorption. On the other hand, for pulses with area equal to even multiples of  $\pi$ , the solutions are stable [27] and the pulses should continue to propagate as solitons through the resonant medium. Throughout the simulations, initial population profile corresponding to the case of an absorbing medium (i.e., all resonant dipoles are initially in the ground state so that  $S_7 = S_{7e} = -1$ ) is assumed. The pulse initially propagates in a free-space region, then enters the degenerate three-level medium, and finally exits the medium into another free-space region. The entire simulation region is taken to be a rectangle  $N_{\text{cells}}$  long and  $M_{\text{cells}}$  wide. In this particular case,  $N_{\text{cells}} = 5000$ ,

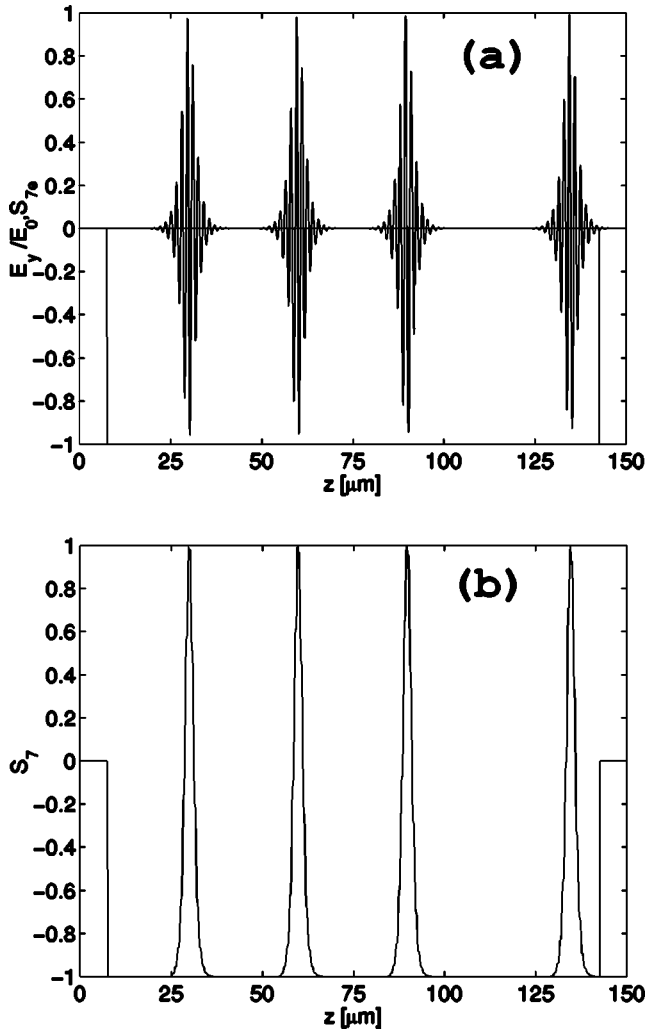


FIG. 3. (a) Spatial profile (along the propagation axis  $z$ ) of the normalized field component  $E_y$  for a HS pulse with initial pulse area equal to  $2\pi$  (maximum amplitude  $E_0 = 4.2186 \times 10^9$  V/m) at the simulation times  $t = 150, 250, 350,$  and  $500$  fs. (b) Population term  $S_7$  profile along the propagation direction at the simulation times of (a). The simulation region is  $150 \mu\text{m}$  long and  $50 \mu\text{m}$  wide and the active (absorbing) medium extends from  $7.5$  to  $142.5 \mu\text{m}$ .

$M_{\text{cells}} = 100$ . An initial pulse with carrier frequency  $\omega_0$  equal to the atomic resonance frequency and with a hyperbolic-secant envelope starts to propagate from the lower boundary (at  $z = 0$ ). The pulse duration is  $T_p = 100$  fs and the maximum field amplitude  $E_0$  is calculated according to the pulse area theorem:

$$E_0 = \frac{2\pi\hbar f_0}{\varphi \arctan(\sinh(u)) \Big|_{-10}^{+10}} \frac{\theta_{\text{pulse}}(z=0)}{2\pi}. \quad (43)$$

In the above equation, all parameters are assigned the values discussed in Sec. III. The step sizes along the  $z$  and  $y$  directions have been chosen as  $\Delta z = 30$  and  $\Delta y = 500$  nm, respectively. Applying the Courant stability criterion, one finds the time step  $\Delta t = 9.989 \times 10^{-2}$  fs. The simulation region is  $150 \mu\text{m}$  long and  $50 \mu\text{m}$  wide.

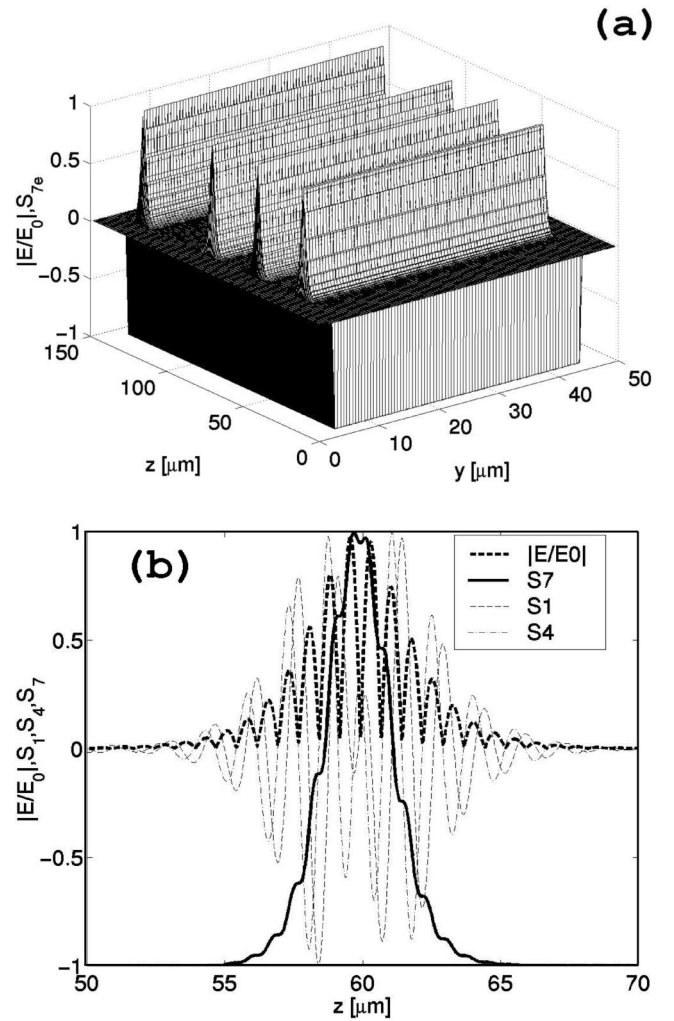


FIG. 4. (a) Modulus of the electric field for the  $\text{TM}_0$  parallel-plate mirror guided mode (TEM plane wave) as a function of the point  $(y, z)$  in the waveguide plane at the simulation times  $t = 150, 250, 350,$  and  $500$  fs. The initial population profile  $S_{7e}$  is included as an indication of the 2D boundaries of the active medium. (b) Cross section of the 3D plots of the normalized electric-field modulus, the in-phase (or dispersive) polarization components  $S_1$ , in-quadrature (or absorptive) polarization component  $S_4$ , the population inversion term  $S_7$  in plane perpendicular to the waveguide, and passing through the middle of the transverse dimension of the waveguide as a function of the longitudinal coordinate  $z$ .

The stable solution case is depicted in Figs. 3(a) and 3(b), where the pulse area is calculated from Eq. (43) and is taken to be  $2\pi$ , leading to a pulse amplitude  $E_0 = 4.2186 \times 10^9$  V/m. In Fig. 3(a), the normalized field component  $E_y$  is plotted against the distance along the structure at the times  $t = 150, 250, 350,$  and  $500$  fs. It can be clearly seen that the initial  $2\pi$  pulse propagates in the resonant medium maintaining its hyperbolic-secant shape without any distortions. The corresponding population difference experiences a complete transition from its ground level to the excited state and back to its initial state within one Rabi period [Fig. 3(b)].

In the case of an initial pulse area less than  $\pi$ , the initially symmetrical pulse shape is distorted during its propagation

in the active medium. The initial equilibrium between the energy absorbed during the leading fraction of the pulse and the energy emitted back to the pulse by stimulated emission within the trailing fraction of the pulse is broken, and the pulse becomes more and more asymmetric. Initially, the leading fraction of the pulse is gradually damped while the trailing irradiated edge grows continuously and is transmitted eventually through the lower ( $z=0$ ) perfectly transmitting boundary. This process persists until the pulse amplitude completely vanishes as the pulse is absorbed by the medium. At the same time, the active medium is only partially inverted, and the pulse energy is not sufficient to induce a full Rabi flop from the ground state to the excited state, and back to the ground state. Therefore, the pulse never reaches dynamical equilibrium. This solution becomes unstable; and, eventually within many absorption lengths in the medium, it decays to zero.

It is straightforward to show that the TEM guided mode case is in turn equivalent to the TE case. At the end of Sec. II C we showed that the TE guided mode is equivalent to a 1D two-level system and that the real state vector components in this case having a clear physical meaning are  $S_1$ ,  $S_4$ , and  $S_7$ . These components represent, respectively, the in-phase (dispersive) component of the polarization, the in-quadrature (absorptive) polarization component, and the population difference in the populations of the two levels (the upper being doubly degenerate). Numerically, this property of the Maxwell-Bloch system manifests itself by a natural splitting of the system of equations for the real-vector components into two sets. As shown in Sec. II C, the first set involves the components corresponding to the two-level system, which are coupled by the TEM mode; while the rest of the equations include transitions involving the third level, which are not coupled by the TEM mode.

The time evolution of the spatial distribution of the modulus of the electric field at four time moments ( $t=150, 250, 350,$  and  $500$  fs) after the plane wave has started its propagation from the boundary  $z=0$  and a cross section of the polarization vector components and the population difference in the 2D TEM mode along the propagation axis are shown in Figs. 4(a) and 4(b). The modulus of the electric-field distribution is plotted together with the initial population profile in Fig. 4(a). The latter has been initially set to  $S_{7e} = -1$  within the active region and zero outside it, and corresponds to an absorbing medium. The leading edge of the electric-field SIT  $2\pi$  pulse completely excites the degenerate three-level quantum system locally, and the trailing edge deexcites it back to the ground state, thereby returning back to the pulse by stimulated emission (during the last half of the pulse), the excitation energy acquired by the system during the first half of the pulse. Therefore, the simulation results for a 2D TEM guided wave propagation across a degenerate three-level system of resonant absorbers correctly reproduces the results from Ref. [9] for SIT-soliton propagation in 1D for a two-level system.

In order to complete our study, we validated our 2D model against the predictions of the pulse area theorem for the time evolution of an arbitrary shaped pulse (e.g., Gaussian) with initial pulse area  $\pi < \theta_{\text{pulse}}(z=0) < 2\pi$ . According

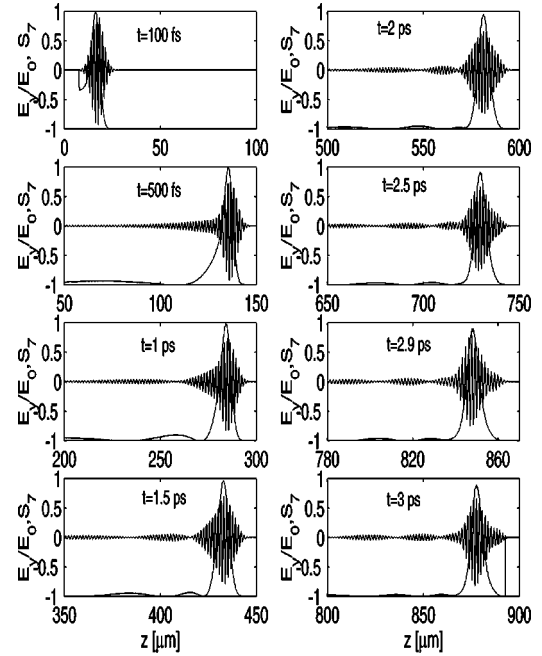


FIG. 5. Cross section of the spatial distribution of the normalized  $E_y$  component and of the population difference term  $S_7$  distribution along the propagation axis  $z$  through the middle of the transverse waveguide dimension at the simulation times  $t=0.1, 0.5, 1, 1.5, 2, 2.5, 2.9,$  and  $3$  ps showing the pulse reshaping during the propagation in the absorbing medium.

to the theorem, a pulse with initial pulse area in the interval  $(\pi, 2\pi)$  should evolve into a SIT  $2\pi$  soliton with hyperbolic-secant envelope [27]. In order to prove this statement, we have performed the following numerical experiment. Using the same geometry for the simulation region as in the previous simulations ( $N_{\text{cells}}=30\,000$ ,  $M_{\text{cells}}=100$ ,  $\Delta z=30$  nm,  $\Delta y=500$  nm, and  $\Delta t=9.989 \times 10^{-2}$  fs), we have injected into the active region a Gaussian pulse with initial pulse area of  $1.6\pi$ . This area and a pulse temporal width  $T_p=100$  fs yields the source electric-field amplitude  $E_0=2.114\,79 \times 10^9$  V/m. The time evolution of the pulse shape has been monitored at evenly spaced time intervals. Figure 5 represents a cross section of the 3D distribution of the normalized  $y$  component of the electric field along the propagation direction through the middle of the transverse dimension plotted together with the corresponding population profile. The actual pulse reshaping during the propagation in the absorbing medium due to the absorption of the leading edge of the pulse and stimulated emission induced by the trailing edge is clearly seen. This absorption results in a broadened, increasingly symmetric  $2\pi$  pulse with HS envelope at the end of the active region, propagating in the absorbing medium without any distortions as a solitary wave.

Finally, as additional evidence in support of the hypothesis that ultrashort pulse propagation in 2D through a degenerate three-level system of quantum absorbers results in a solitonlike behavior, we have performed a numerical experiment that demonstrates the soliton interaction. It is well known that when solitons interact with each other, they re-emerge after the interaction with unchanged shape and only

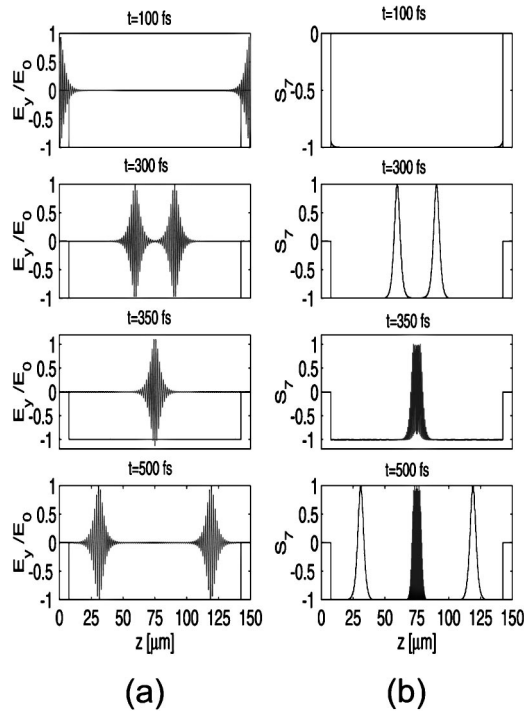


FIG. 6. (a) Normalized  $E_y$ -component  $z$  distribution (obtained as a cross section of the 3D plot through the middle point of the transverse waveguide dimension) of two counterpropagating  $2\pi$  pulses with Gaussian envelope ( $\tau=200$  fs,  $E_0=2.1093 \times 10^9$  V/m) at the simulation times  $t=100$ , 300, 350, and 500 fs. At a time  $t=350$  fs, the two pulses interact; the interaction manifests itself as a summation of the pulse amplitudes. After the interaction, the pulses restore their original shape and continue to propagate as solitary waves. (b) Cross section of the 3D plot of the population term  $S_7$  at the same simulation times, reflecting the population disturbance caused by the pulse interaction (memory effect at the point of encounter of the two pulses).

with a shift in their phase (see, e.g., Ref. [29]). In our numerical simulations, we have applied two electric-field sources, each located at opposite ends of the simulation region, which have the HS shape and initial area equal to  $2\pi$  (i.e.,  $E_0=2.1093 \times 10^9$  V/m,  $\tau=200$  fs). The results of the simulations for the time evolution of the normalized electric-field component  $E_y$  are plotted in Fig. 6(a), and the population difference is plotted in Fig. 6(b) together with the boundaries of the active region. The two counterpropagating pulses interact in the middle of the simulation region; this effectively results in a summation of their amplitudes. After the interaction the two pulses, they reappear without any changes in their shape and maintain their soliton character [Fig. 6(a)]. The population difference term  $S_7$  exhibits strong oscillations during the interaction and also reappears after the interaction, as it has been before.

### B. $\text{TM}_1$ guided mode SIT soliton

Let us consider now the more complicated and interesting case of propagation of the  $\text{TM}_1$  guided mode in a parallel-plate mirror waveguide through a degenerate three-level sys-

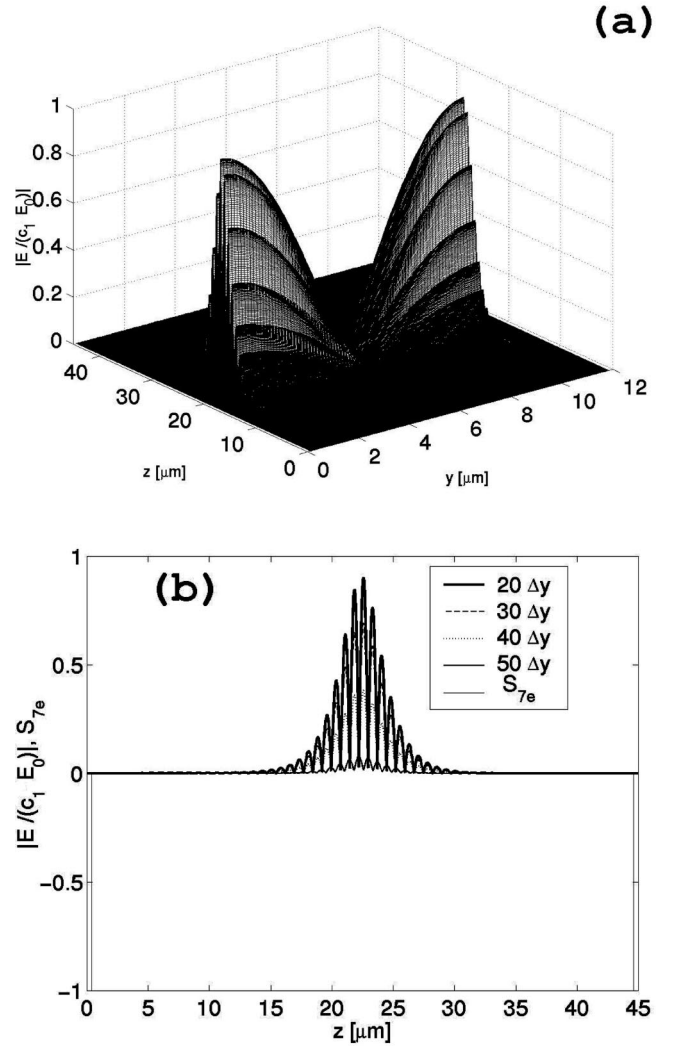


FIG. 7. Normalized optical field distribution of the first-order ( $\text{TM}_1$ ) mode of the parallel-mirror waveguide: (a) Absolute value of the normalized electric-field distribution at a time  $t=125$  fs; (b) Cross section of the normalized modulus of the electric-field profile and the initial population profile  $S_{7e}$  along the waveguide axis at  $y=j\Delta y$  (where  $j=20, 30, 40, 50$ ).

tem of resonant dipoles. In this case the electric field couples all the three levels, and the polarization can be induced both in the propagation direction and in the transverse direction. The purpose of this study is to provide numerical evidence of SIT-soliton existence in two spatial dimensions. This is a nontrivial task; the analytical solutions of the Maxwell-pseudospin system in 2D are not known. The problem is rendered even more difficult from a mathematical point of view because of the presence of the relaxation (damping) terms.

The geometry of the simulation region is assumed to be the same as for the previous TEM ( $\text{TM}_0$ ) case. The pulse initially propagates in a free-space region, and thereafter enters the active medium; the pulse subsequently continues to propagate in the nonlinear medium and exits into a free-space region again. The number of cells along the propagation direction is  $N_{\text{cells}}=30\,000$ , and in the transverse direc-

tion  $M_{\text{cells}}=100$ . Since we do not have any knowledge about the stable solution pulse envelope, we make an initial assumption for the pulse shape and start to propagate a  $2\pi$  pulse (HS) from the lower boundary ( $z=0$ ) with maximum electric-field amplitude  $E_0$ , normalized with respect to the amplitude  $c_1$  of the  $E_y$  TM<sub>1</sub> mode of the parallel-plate mirror optical waveguide [see, e.g., Ref. [26], Eq. (39)]. For the parameter set used in the simulations, with refractive index of the active medium being  $n=1$  and the separation between the side mirrors being  $d=9.9185\ \mu\text{m}$ , we obtained a value of  $c_1=375.652$ , resulting in maximum field amplitude  $E_0=1.123\times 10^7\ \text{V/m}$ . The step sizes  $\Delta z=1.5\ \text{nm}$  along the  $z$  direction and  $\Delta y=119.5\ \text{nm}$  along the  $y$  direction were chosen. The resulting time step, according to the Courant condition in 2D [Eq. (40)], was set to  $\Delta t=5\times 10^{-3}\ \text{fs}$ . A snapshot of the 3D absolute value of the electric-field distribution at a time  $t=125\ \text{fs}$  is plotted in Fig. 7(a). The corresponding cross section along the propagation axis at point of the transverse dimension  $y_j=j\Delta y$  ( $j=20, 30, 40, 50$ ) is given in Fig. 7(b) along with the initial population profile  $S_{7e}$ . In this simulation we assumed an absorbing medium and, therefore, set the equilibrium population terms to their equilibrium values [i.e.,  $S_{7e}=-1$  and  $S_{8e}=-(1/\sqrt{3})$ ]. Instead of plotting all the eight real pseudospin vector components, we have plotted only the significant polarization components, corresponding to actual transitions that occur in the degenerate three-level system and the level-occupation probabilities (diagonal elements in the density matrix), since the latter provide more immediate insight into the population redistribution between the levels in the three-level system considered. The significant polarization components are plotted in Figs. 8(a–h) as a 3D plot and are viewed in a plane perpendicular to the plane of the simulation structure, that intersects the transverse dimension at particular distances from the lower interface. In Figs. 8(a,b) and Figs. 8(e,f), the polarization components  $S_1$  and  $S_4$  are plotted; they show a behavior similar to the respective components in the TEM case [compare with Fig. 4(b)]. By inspecting Fig. 8, it can be seen that the behavior of the coherence vector components is very similar to the following pairs of components:  $S_1$  and  $S_4$  (representing the in-phase and in-quadrature components of the polarization, respectively), and  $S_3$  and  $S_6$ . This is due to the fact that these pairs of components are responsible [see Eq. (34)] for the coupling between the levels 1 and 2, and 1 and 3, respectively. The level-occupation probabilities are plotted in Figs. 9(a–d). From the cross-section plot given in Figs. 9(b–d) [a similar behavior of the population difference as for the TEM mode, i.e., compare with Fig. 4(b)], the SIT behavior is discerned clearly, namely, the population is totally inverted and returned back to the ground-state population by the pulse, thereby performing one Rabi flop. Figure 9(a) shows two transitions, i.e., two Rabi flops, of the population difference from the ground state to the excited state, and back along the transverse direction. For each of these transverse Rabi flops, a corresponding Rabi flop occurs along the propagation axis; this behavior reflects the symmetry of the mode. However, level 3 is maintained partially populated during the pulse propagation. The behavior of the level-occupation probabilities is an indication of the presence of

the self-induced transparency effects.

In Figs. 10(a–d), we have plotted a snapshot of the spatial distribution of the normalized  $E_y$  and  $E_z$  components of the electric field at three time moments ( $t=90, 125, 155\ \text{fs}$ ) during the propagation of the pulse in the active medium. For both components of the incident field, the maximum field amplitudes have been chosen to correspond to a  $2\pi$  SIT-soliton pulse. In particular, by virtue of the pulse area theorem,  $E_0=4.2186\times 10^9\ \text{V/m}$  at the lower boundary ( $z=0$ ), and this value is subsequently normalized with respect to the amplitude coefficient  $c_1$  of the parallel-plate mirror waveguide TM<sub>1</sub> mode. Justification of this normalization procedure is given below. It is clear from this figure that the electric-field components maintain their shape during the propagation in the nonlinear medium. This can be discerned clearly from Figs. 10(b,d) representing plots of the cross section along the propagation axis. The corresponding time evolution of the level-occupation probabilities is shown in Fig. 11. These results thus indicate that a solitonlike regime of ultrashort pulse propagation has been achieved even for the TM<sub>1</sub> mode when the field couples to all three levels in the system.

### C. Pulse area theorem generalization to multidimensions

From the above numerical evidence of the existence of solitonlike behavior in a two-dimensional resonant degenerate three-level medium, we can restate and extend the general result of the pulse area theorem in more than one spatial dimension. In what follows, we shall show that the choice of the maximum electric-field amplitude  $E_0$  that results in a solitonlike behavior of the TM<sub>1</sub> mode simulation case is a consequence of this more general requirement.

For a generic TM<sub>1</sub> wave, the pulse area along the propagation axis can be defined as

$$\theta(y=y_0, z) = \frac{\varrho}{\hbar} \int_{-\infty}^{\infty} \tilde{E}_y(y_0, z, t') dt', \quad (44)$$

where the envelope  $\tilde{E}_y(y, z, t') = E_0 c_1 \cos(\pi y/d) \text{sech}[(t' - z/V_z)/\tau]$ ,  $V_z$  is the component of the pulse group velocity along the propagation axis, and the constant  $c_1$  is given by Eq. (39). Similarly, we can define the pulse area along the  $z$  direction for the  $E_z$  component:

$$\theta(y=y_0, z) = \frac{\varrho}{\hbar} \int_{-\infty}^{\infty} \tilde{E}_z(y_0, z, t') dt', \quad (45)$$

where the envelope  $\tilde{E}_z(y, z, t') = -E_0 c_2 \sin(\pi y/d) \text{sech}[(t' - (z/V_z)]/\tau]$ . We then define a pulse area under the absolute value of the field envelope  $|\tilde{E}(y, z, t')| = \sqrt{\tilde{E}_y^2(y, z, t') + \tilde{E}_z^2(y, z, t')}$  as

$$\theta(y, z) = \frac{\varrho}{\hbar} \int_{-\infty}^{\infty} |\tilde{E}(y, z, t')| dt' = \frac{\varrho}{\hbar} \int_{-\infty}^{\infty} \sqrt{\tilde{E}_y^2 + \tilde{E}_z^2} dt'. \quad (46)$$

Substituting the field envelopes from Eq. (39), we find that the initial pulse area injected into the active medium at a point  $y=y_0$  is obtained as follows:

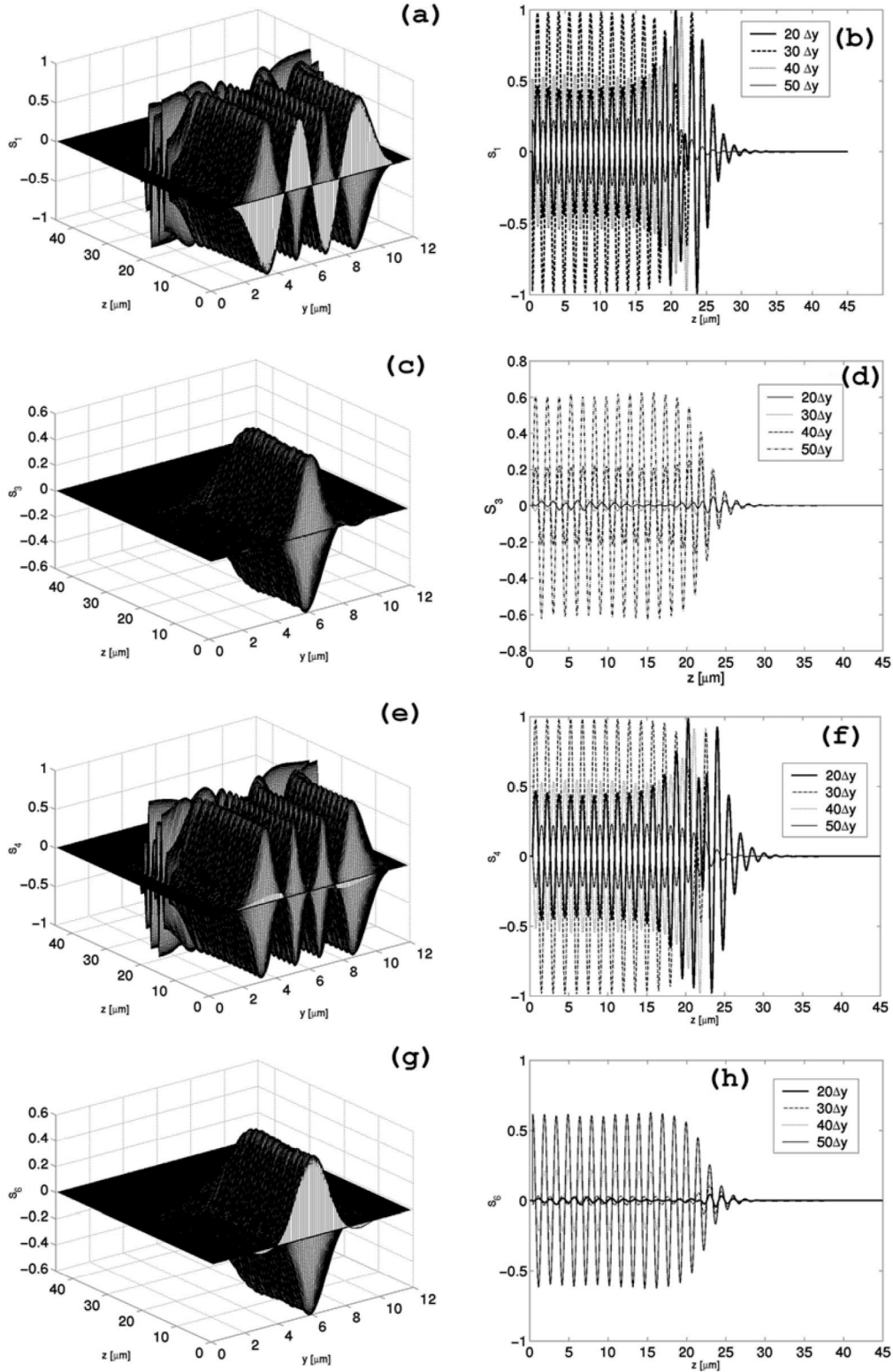


FIG. 8. Plot of the significant polarization components  $S_1$ ,  $S_3$ ,  $S_4$ ,  $S_6$  for the  $\text{TM}_1$  mode: (a) Polarization component  $S_1$  as a function of the in-plane coordinates at a simulation time  $t = 125$  fs during the propagation in the active region. (b) Cross section of  $S_1$  at  $y_j = j\Delta y$  (where  $j = 20, 30, 40, 50$ ). (c) Polarization component  $S_3$  as a function of the in-plane coordinates at a simulation time  $t = 125$  fs during the propagation in the active region. (d) Cross section of  $S_3$  at  $y_j = j\Delta y$  (where  $j = 20, 30, 40, 50$ ). (e) Polarization component  $S_4$  as a function of the in-plane coordinates at a simulation time  $t = 125$  fs during the propagation in the active region. (f) Cross section of  $S_4$  at  $y_j = j\Delta y$  (where  $j = 20, 30, 40, 50$ ). (g) Polarization component  $S_6$  as a function of the in-plane coordinates at a simulation time  $t = 125$  fs during the propagation in the active region. (h) Cross section of  $S_6$  at  $y_j = j\Delta y$  (where  $j = 20, 30, 40, 50$ ).

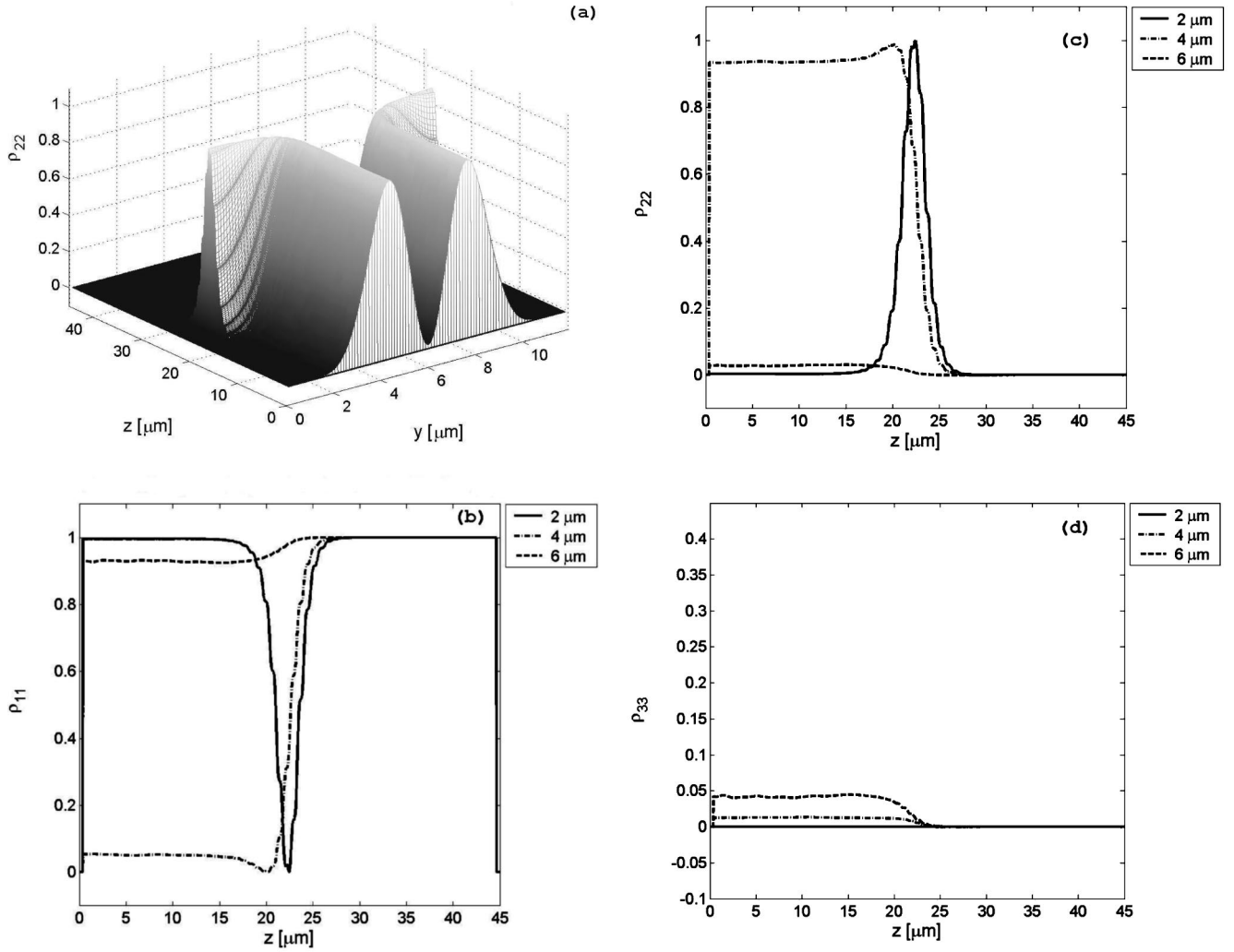


FIG. 9. Level-occupation probabilities ( $\rho_{11}$ ,  $\rho_{22}$ , and  $\rho_{33}$ ) for the  $TM_1$  mode in a degenerate three-level system: (a) Occupation probability for level 2 as a function of the in-plane coordinates at a simulation time  $t=125$  fs during the propagation in the active region. (b) Cross section of occupation probability for level 1 ( $\rho_{11}$ ) at  $y=2, 4, 6 \mu\text{m}$  from the lower interface (note that  $\rho_{11}$  exhibits the same characteristics as the plot of  $S_7$  component of the TEM mode [Fig. 4(b)]). (c) Cross section of occupation probability for level 2 ( $\rho_{22}$ ) at  $y=2, 4, 6 \mu\text{m}$  from the left ( $y=0$ ) interface. (d) Cross section of occupation probability for level 3 ( $\rho_{33}$ ) at  $y=2, 4, 6 \mu\text{m}$  from the left ( $y=0$ ) interface.

$$\begin{aligned}
 \theta(y_0, z=0) &= \frac{\wp}{\hbar} E_0 c_1 \left[ \cos^2\left(\frac{\pi y_0}{d}\right) \right. \\
 &\quad \left. + \left(\frac{c_2}{c_1}\right)^2 \sin^2\left(\frac{\pi y_0}{d}\right) \right]^{1/2} \int_{-\infty}^{\infty} \text{sech}\left(\frac{t'}{\tau}\right) dt' \\
 &= \frac{\wp}{\hbar} E_0 c_1 \left[ \cos^2\left(\frac{\pi y_0}{d}\right) + \left(\frac{c_2}{c_1}\right)^2 \sin^2\left(\frac{\pi y_0}{d}\right) \right]^{1/2} \pi \tau.
 \end{aligned} \tag{47}$$

It is straightforward to see that for  $y_0=0$  and  $y_0=d$ , we obtain an initial pulse area that corresponds to the one obtained in the 1D setting [see Eq. (43)], with a factor of  $c_1$  in excess, namely,

$$\begin{aligned}
 \theta(y_0=0, z) &= \theta(y_0=d, z) = \frac{\wp}{\hbar} E_0 c_1 \pi \tau = 4 \pi^2 \frac{\wp}{\hbar \omega_0} E_0 c_1 \\
 &= c_1 \theta_{1D}.
 \end{aligned} \tag{48}$$

Therefore we can calculate the maximum field amplitude again from Eq. (43) multiplied by an additional factor  $c_1$ . This leads in turn to a value  $E_0 = (4.2186 \times 10^9)/c_1$  V/m. In fact, this is the value used in the simulations of the  $TM_1$  mode case. This result establishes a novel criterion in 2D for obtaining solitonlike behavior that is based on the area under the modulus of the electric-field envelope.

## V. CONCLUSIONS

The present approach for the semiclassical treatment of resonant coherent interactions in a degenerate three-level

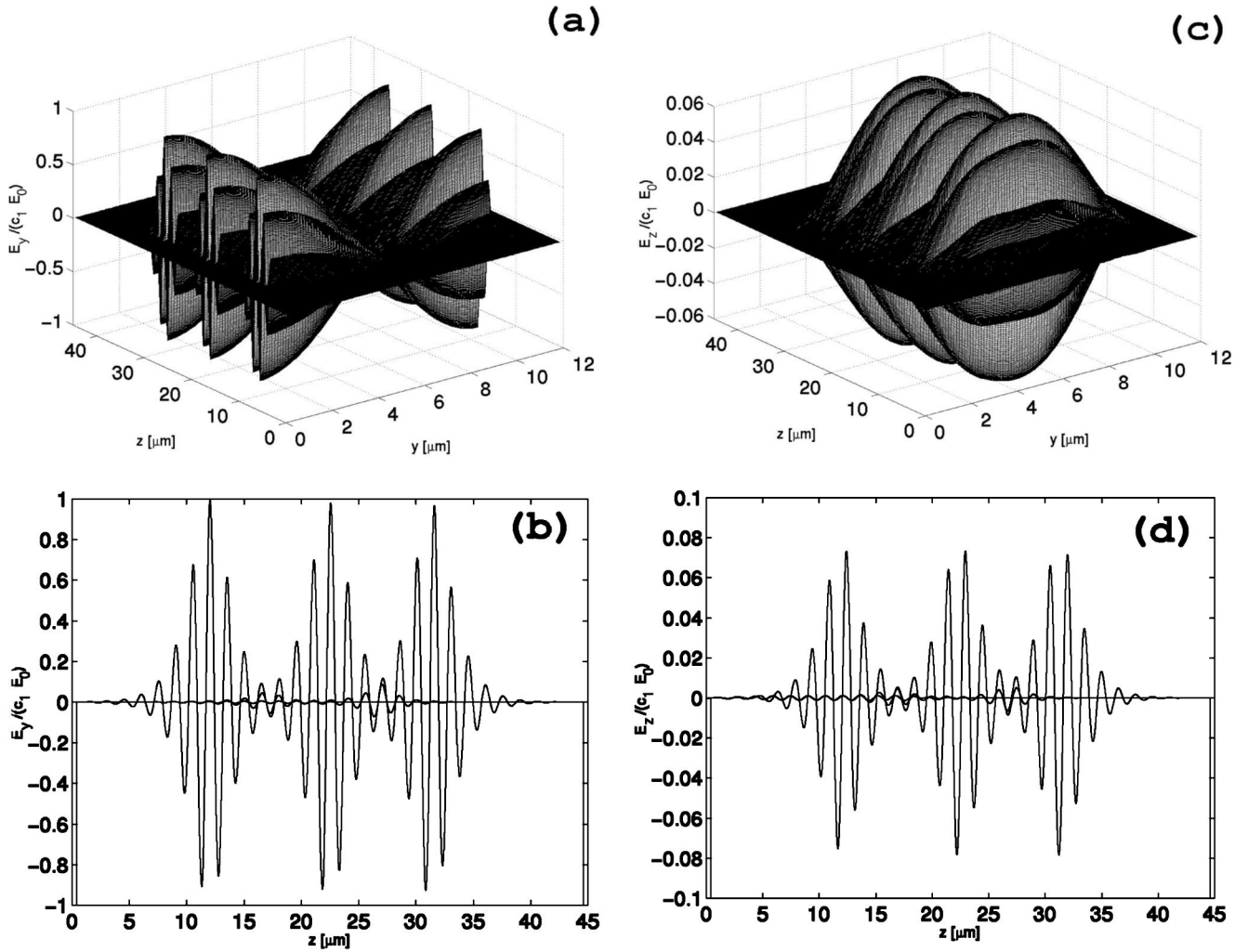


FIG. 10. Evolution of the optical field distribution for the  $\text{TM}_1$  mode at the simulation times  $t=90, 125,$  and  $155$  fs showing the conservation of the 2D-pulse shape during the propagation in the absorbing medium: (a) Normalized  $E_y$  component of the optical field as a function of the in-plane coordinates. (b) Cross section of the 3D profile of  $E_y$  along the propagation direction at a point  $y=10\Delta y$  along with the cross section of the initial population profile  $S_{7e}$ , showing the boundaries of the active region along  $z$ . (c) Normalized  $E_z$ -component as a function of the in-plane coordinates. (d) Cross section of the 3D profile of  $E_z$  along the propagation direction at a point  $y=10\Delta y$  along with the cross section of the initial population profile  $S_{7e}$ , showing the boundaries of the active region along  $z$ .

system in 2D represents a generalization of the Maxwell-Bloch equations for a two-level system. The model properly accounts through the polarization sources in Maxwell's equations for the polarizations of the three-level medium in 2D, which generally occur along two perpendicular directions. The advantage of the newly derived set of linear differential equations is a direct consequence of the real-vector representation model (rather than a complex density-matrix approach). It represents a simple but rigorous geometrical picture of the resonance behavior of the quantum system with clear physical meaning of the quantities involved. This approach in turn allows a relatively easy numerical implementation. The set of equations have been discretized on a specially constructed modified 2D Yee grid and solved directly in the time domain (by generalizing the predictor-corrector method to a three-level system and two spatial dimensions).

We have applied the approach based on the Maxwell-pseudospin system to the study of the TE and TM modes in

a parallel-plate mirror optical waveguide loaded with a degenerate three-level quantum system. The main physical implications from our studies can be summarized as follows. We have confirmed from a different Maxwell-pseudospin system that the SIT effects can be recovered in the quasi-1D case, i.e., the 2D  $\text{TM}_0$  (TEM) mode case. Most importantly, novel physical effects including 2D solitary wave and SIT behavior were obtained with this multidimensional Maxwell-pseudospin system. The results for the SIT soliton associated with the  $\text{TM}_1$  mode are of particular interest since these demonstrate SIT effects and solitonlike behavior in 2D in an irreducible three-level quantum system. A generalization of the pulse area theorem was postulated and validated numerically, which accounts for the multidimensionality of the electromagnetic wave and the polarization dynamics of the quantum system.

The proposed model provides a useful and powerful tool for the investigation of the population dynamics during the

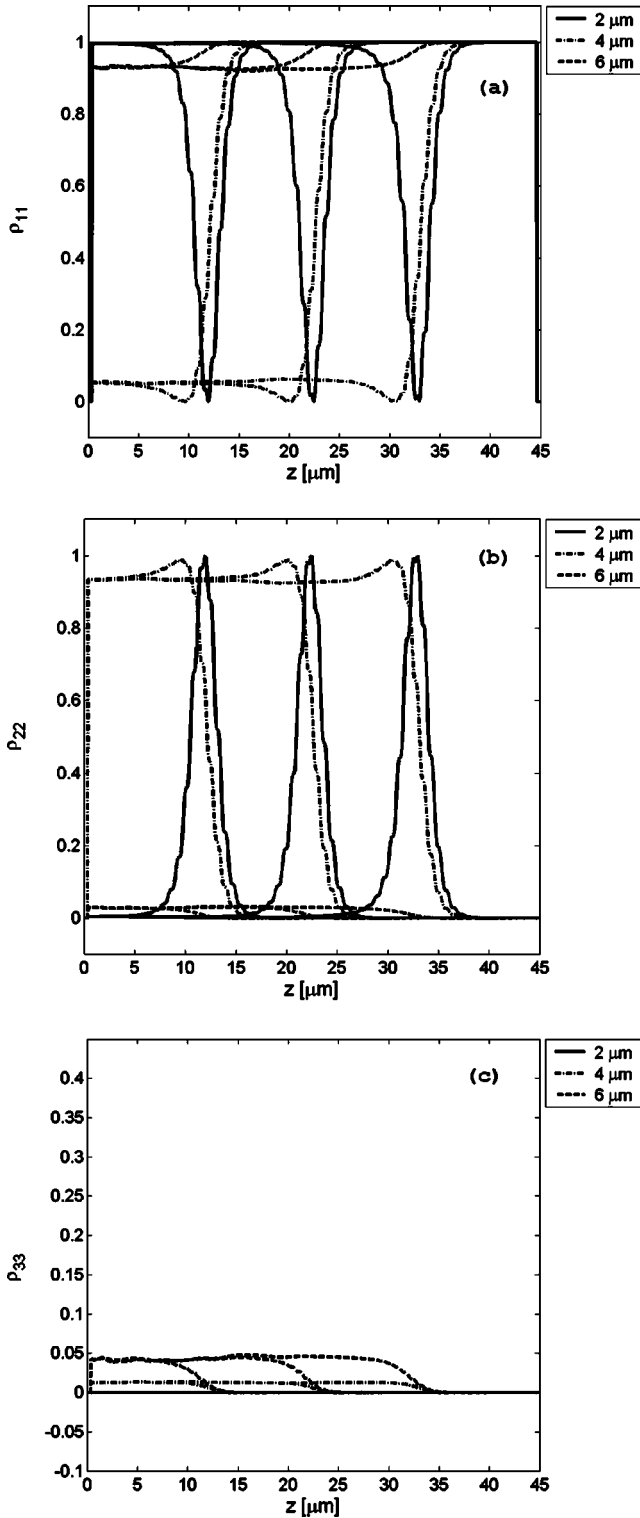


FIG. 11. Evolution of the level-occupation probabilities ( $\rho_{11}$ ,  $\rho_{22}$ , and  $\rho_{33}$ ) for the  $TM_1$  mode in a degenerate three-level system at the simulation times  $t=90$ ,  $125$ , and  $160$  fs: (a) Cross section of the 3D plot of the occupation probability for level 1 ( $\rho_{11}$ ) at  $y=2, 4, 6 \mu\text{m}$  from the left ( $y=0$ ) interface. (b) Cross section of  $\rho_{22}$  at  $y=2, 4, 6 \mu\text{m}$  from the left ( $y=0$ ) interface. (c) Cross section of  $\rho_{33}$  at  $y=2, 4, 6 \mu\text{m}$  from the left ( $y=0$ ) interface.

propagation of ultrashort 2D electromagnetic pulses through a multilevel quantum system, and we are anticipating using it in the extreme nonlinear regime in the future.

It is to be noted that in the simulated parallel-plate mirror optical waveguide configuration, the TE and TM modes have the same propagation coefficients. This in turn leads to a solitonlike behavior of the total wave for both types of modes. It is, however, worthwhile to investigate the critical conditions for the occurrence of mixed  $TE_1/TM_1$  modes that would in turn allow for the formation of polarized solitons. The latter would require considerations of a four-level system and an extension of the above formalism to the  $SU(4)$  group. This possibility is currently under investigation and will be reported in a future publication.

#### ACKNOWLEDGMENTS

One of the authors (G.S.) would like to acknowledge the EPSRC project PHOTON, under which the work has been carried out and the CPU time on the parallel multiprocessor station at the department under VIDEOS project funded by SHEFC research development grant. Stimulating discussions with K. Bubke and D. Modotto are gratefully acknowledged.

#### APPENDIX: DISCRETIZATION OF THE MAXWELL-BLOCH EQUATIONS FOR THE TRANSVERSE MAGNETIC WAVE

We apply the standard staggered-grid finite-difference scheme of the spatial and temporal derivatives into the continuum equations (35c) and (35d) for the transverse magnetic wave in 2D. The electric-field components and the magnetic-field components are spatially separated by  $\Delta y/2$  and  $\Delta z/2$  in  $y$ - $z$  plane and temporally by  $\Delta t/2$ . The  $E$  components are situated in the middle of the edges, and the  $H$  components are in the center of the cell [25]. We associate the quantum system variables with the empty nodes in the 2D Yee grid, providing electric-field values at these mesh points by averaging over the electric fields located at the nearest neighbors in the plane of a given node. The averaging procedure is explicitly given below.

As has been pointed out in Ref. [9], the exponential decaying terms make the Bloch equation numerically stiff, therefore additional analytical factoring out of the exponential dependence is necessary before discretizing them. Similar to Ref. [9], we introduce the new variables  $u_i$  ( $i=1,2,\dots,8$ ) according to

$$S_i(y, z, t) = \exp(-t/T_1)u_i(y, z, t), \quad i=1, 2, \dots, 6,$$

$$S_7(y, z, t) = S_{7e} + \exp(-t/T_7)u_7(y, z, t), \quad (\text{A1})$$

$$S_8(y, z, t) = S_{8e} + \exp(-t/T_8)u_8(y, z, t).$$

The resulting set of equations acquires the form

$$\frac{\partial H_x}{\partial t} = -\frac{1}{\mu} \frac{\partial E_z}{\partial y} + \frac{1}{\mu} \frac{\partial E_y}{\partial z},$$

$$\frac{\partial E_y}{\partial t} = \frac{1}{\epsilon} \frac{\partial H_x}{\partial z} - A_y u_1 - B_{y4} u_4 - B_{y5} u_5, \quad (\text{A2})$$

$$\begin{aligned}
\frac{\partial E_z}{\partial t} &= -\frac{1}{\varepsilon} \frac{\partial H_x}{\partial y} - A_z u_3 - B_{z5} u_5 - B_{z6} u_6; \\
\frac{\partial u_1}{\partial t} &= -\omega_0 C_{14+} u_4 - C_{15+} E_z u_5, \\
\frac{\partial u_2}{\partial t} &= C_{24+} E_z u_4 + C_{26+} E_y u_6, \\
\frac{\partial u_3}{\partial t} &= C_{35+} E_y u_5 - \omega_0 C_{36+} u_6, \\
\frac{\partial u_4}{\partial t} &= \omega_0 C_{14-} u_1 - C_{24-} E_z u_2 - D_{74} E_y - C_{47+} E_y u_7, \\
\frac{\partial u_5}{\partial t} &= C_{15-} E_z u_1 - C_{35-} E_y u_3, \\
\frac{\partial u_6}{\partial t} &= -C_{26-} E_y u_2 + \omega_0 C_{36-} u_3 - D_{76} E_z - C_{67+} E_z u_7 \\
&\quad - D_{86} E_z - C_{68+} E_z u_8, \\
\frac{\partial u_7}{\partial t} &= C_{47-} E_y u_4 + C_{67-} E_z u_6, \\
\frac{\partial u_8}{\partial t} &= C_{68-} E_z u_6, \tag{A3}
\end{aligned}$$

$$\begin{aligned}
B_{y5}(t) &= \frac{N_a \wp^2}{\hbar \varepsilon} \exp(-t/T_5), \\
C_{26\pm}(t) &= \frac{\wp}{\hbar} \exp[\pm t((1/T_2) - (1/T_6))], \\
B_{z5}(t) &= \frac{N_a \wp^2}{\hbar \varepsilon} \exp(-t/T_5), \\
C_{35\pm}(t) &= \frac{\wp}{\hbar} \exp[\pm t((1/T_3) - (1/T_5))], \\
B_{z6}(t) &= \frac{N_a \wp \omega_0}{\varepsilon} \exp(-t/T_6), \\
C_{36\pm}(t) &= \exp[\pm t((1/T_3) - (1/T_6))], \\
C_{47\pm}(t) &= \frac{2\wp}{\hbar} \exp[\pm t((1/T_4) - (1/T_7))], \\
C_{67\pm}(t) &= \frac{\wp}{\hbar} \exp[\pm t((1/T_6) - (1/T_7))], \\
C_{68\pm}(t) &= \frac{\sqrt{3}\wp}{\hbar} \exp[\pm t((1/T_6) - (1/T_8))], \\
D_{74}(t) &= \frac{2\wp}{\hbar} S_{7e} \exp(t/T_4), \\
D_{76}(t) &= \frac{\wp}{\hbar} S_{7e} \exp(t/T_6), \\
D_{86}(t) &= \frac{\sqrt{3}\wp}{\hbar} S_{8e} \exp(t/T_6). \tag{A4}
\end{aligned}$$

where the following time-varying coefficients have been defined:

$$\begin{aligned}
A_y(t) &= \frac{N_a \wp}{\varepsilon T_1} \exp(-t/T_1), \\
C_{14\pm}(t) &= \exp[\pm t((1/T_1) - (1/T_4))], \\
A_z(t) &= \frac{N_a \wp}{\varepsilon T_3} \exp(-t/T_3), \\
C_{15\pm}(t) &= \frac{\wp}{\hbar} \exp[\pm t((1/T_1) - (1/T_5))], \\
B_{y4}(t) &= \frac{N_a \wp \omega_0}{\varepsilon} \exp(-t/T_4), \\
C_{24\pm}(t) &= \frac{\wp}{\hbar} \exp[\pm t((1/T_2) - (1/T_4))],
\end{aligned}$$

With the locations of the discrete variables assumed above, the magnetic-field equation is solved at the space steps  $(i + \frac{1}{2})\Delta z$  and  $(j + \frac{1}{2})\Delta y$  for time steps  $(k + \frac{1}{2})\Delta t$ . The field components  $E_y$  and  $E_z$  are solved correspondingly at the space steps  $i\Delta z$  and  $(j + \frac{1}{2})\Delta y$ , and  $(i + \frac{1}{2})\Delta z$  and  $j\Delta y$  at a time step  $k\Delta t$ . As a result, a discretized version of the 2D Maxwell-pseudospin system is developed of the following form:

$$\begin{aligned}
H_x\left(i+\frac{1}{2}, j+\frac{1}{2}, k+\frac{1}{2}\right) &= H_x\left(i+\frac{1}{2}, j+\frac{1}{2}, k-\frac{1}{2}\right) - \frac{\Delta t}{\mu\Delta y} \left[ E_z\left(i+\frac{1}{2}, j+1, k\right) - E_z\left(i+\frac{1}{2}, j, k\right) \right] \\
&+ \frac{\Delta t}{\mu\Delta z} \left[ E_y\left(i+1, j+\frac{1}{2}, k\right) - E_y\left(i, j+\frac{1}{2}, k\right) \right], \tag{A5a}
\end{aligned}$$

$$\begin{aligned}
E_y\left(i, j+\frac{1}{2}, k+1\right) &= E_y\left(i, j+\frac{1}{2}, k\right) + \frac{\Delta t}{\varepsilon\Delta z} \left[ H_x\left(i+\frac{1}{2}, j+\frac{1}{2}, k+\frac{1}{2}\right) - H_x\left(i-\frac{1}{2}, j+\frac{1}{2}, k+\frac{1}{2}\right) \right] \\
&- A_1\left(k+\frac{1}{2}\right) \frac{1}{2} \left[ u_1\left(i, j+\frac{1}{2}, k+1\right) + u_1\left(i, j+\frac{1}{2}, k\right) \right] \\
&- B_{14}\left(k+\frac{1}{2}\right) \frac{1}{2} \left[ u_4\left(i, j+\frac{1}{2}, k+1\right) + u_4\left(i, j+\frac{1}{2}, k\right) \right] \\
&- B_{15}\left(k+\frac{1}{2}\right) \frac{1}{2} \left[ u_5\left(i, j+\frac{1}{2}, k+1\right) + u_5\left(i, j+\frac{1}{2}, k\right) \right] \\
&\times \frac{1}{2} \left[ E_z\left(i, j+\frac{1}{2}, k+1\right) + E_z\left(i, j+\frac{1}{2}, k\right) \right], \tag{A5b}
\end{aligned}$$

$$\begin{aligned}
E_z\left(i+\frac{1}{2}, j, k+1\right) &= E_z\left(i+\frac{1}{2}, j, k\right) - \frac{\Delta t}{\varepsilon\Delta y} \left[ H_x\left(i+\frac{1}{2}, j+\frac{1}{2}, k+\frac{1}{2}\right) - H_x\left(i+\frac{1}{2}, j-\frac{1}{2}, k+\frac{1}{2}\right) \right] \\
&- A_2\left(k+\frac{1}{2}\right) \frac{1}{2} \left[ u_3\left(i+\frac{1}{2}, j, k+1\right) + u_3\left(i+\frac{1}{2}, j, k\right) \right] + B_{25}\left(k+\frac{1}{2}\right) \\
&\times \frac{1}{2} \left[ u_5\left(i+\frac{1}{2}, j, k+1\right) + u_5\left(i+\frac{1}{2}, j, k\right) \right] \frac{1}{2} \left[ E_y\left(i+\frac{1}{2}, j, k+1\right) \right. \\
&\left. + E_y\left(i+\frac{1}{2}, j, k\right) \right] - B_{26}\left(k+\frac{1}{2}\right) \frac{1}{2} \left[ u_6\left(i+\frac{1}{2}, j, k+1\right) + u_6\left(i+\frac{1}{2}, j, k\right) \right]. \tag{A5c}
\end{aligned}$$

Pseudospin equations are

$$\begin{aligned}
u_1(i, j, k+1) &= u_1(i, j, k) - \Delta t \omega_0 c_{14+} \left( k+\frac{1}{2} \right) \frac{1}{2} [u_4(i, j, k+1) + u_4(i, j, k)] - \Delta t C_{15+} \\
&\times \left( k+\frac{1}{2} \right) \frac{1}{4} [E_z(i, j, k+1) + E_z(i, j, k)] [u_5(i, j, k+1) + u_5(i, j, k)],
\end{aligned}$$

$$\begin{aligned}
u_2(i, j, k+1) &= u_2(i, j, k) + \Delta t C_{24+} \left( k+\frac{1}{2} \right) \frac{1}{4} [E_z(i, j, k+1) + E_z(i, j, k)] [u_4(i, j, k+1) \\
&+ u_4(i, j, k)] + \Delta t C_{26+} \left( k+\frac{1}{2} \right) \frac{1}{4} [E_y(i, j, k+1) + E_y(i, j, k)] [u_6(i, j, k+1) \\
&+ u_6(i, j, k)],
\end{aligned}$$

$$\begin{aligned}
u_3(i, j, k+1) &= u_3(i, j, k) + \Delta t C_{35+} \left( k+\frac{1}{2} \right) \frac{1}{4} [E_y(i, j, k+1) + E_y(i, j, k)] [u_5(i, j, k+1) + u_5(i, j, k)] \\
&- \omega_0 \Delta t C_{36+} \left( k+\frac{1}{2} \right) \frac{1}{2} [u_6(i, j, k+1) + u_6(i, j, k)],
\end{aligned}$$

$$\begin{aligned}
u_4(i, j, k+1) &= u_4(i, j, k) + \Delta t \omega_0 C_{14-} \left( k + \frac{1}{2} \right) \frac{1}{2} [u_1(i, j, k+1) + u_1(i, j, k)] - \Delta t C_{24-} \left( k + \frac{1}{2} \right) \frac{1}{4} [E_z(i, j, k+1) \\
&\quad + E_z(i, j, k)] [u_2(i, j, k+1) + u_2(i, j, k)] - \Delta t D_{74} \left( k + \frac{1}{2} \right) \frac{1}{2} [E_z(i, j, k+1) + E_z(i, j, k)] \\
&\quad - \Delta t C_{47+} \left( k + \frac{1}{2} \right) \frac{1}{4} [E_y(i, j, k+1) + E_y(i, j, k)] [u_7(i, j, k+1) + u_7(i, j, k)], \\
u_5(i, j, k+1) &= u_5(i, j, k) + \Delta t C_{15-} \left( k + \frac{1}{2} \right) \frac{1}{4} [E_z(i, j, k+1) + E_z(i, j, k)] [u_1(i, j, k+1) + u_1(i, j, k)] \\
&\quad - \Delta t C_{35-} \left( k + \frac{1}{2} \right) \frac{1}{4} [E_y(i, j, k+1) + E_y(i, j, k)] [u_3(i, j, k+1) + u_3(i, j, k)], \\
u_6(i, j, k+1) &= u_6(i, j, k) - \Delta t C_{26-} \left( k + \frac{1}{2} \right) \frac{1}{4} [E_y(i, j, k+1) + E_y(i, j, k)] [u_2(i, j, k+1) + u_2(i, j, k)] \\
&\quad + \Delta t \omega_0 C_{36-} \left( k + \frac{1}{2} \right) \frac{1}{2} [u_3(i, j, k+1) + u_3(i, j, k)] - \Delta t D_{76} \left( k + \frac{1}{2} \right) \frac{1}{2} [E_z(i, j, k+1) + E_z(i, j, k)] \\
&\quad - \Delta t C_{67+} \left( k + \frac{1}{2} \right) \frac{1}{4} [E_z(i, j, k+1) + E_z(i, j, k)] [u_7(i, j, k+1) + u_7(i, j, k)] \\
&\quad - \Delta t D_{86} \left( k + \frac{1}{2} \right) \frac{1}{2} [E_z(i, j, k+1) + E_z(i, j, k)] - \Delta t C_{68+} \left( k + \frac{1}{2} \right) \frac{1}{4} [E_z(i, j, k+1) \\
&\quad + E_z(i, j, k)] [u_8(i, j, k+1) + u_8(i, j, k)], \\
u_7(i, j, k+1) &= u_7(i, j, k) + \Delta t C_{47-} \left( k + \frac{1}{2} \right) \frac{1}{4} [E_y(i, j, k+1) + E_y(i, j, k)] [u_4(i, j, k+1) + u_4(i, j, k)] \\
&\quad + \Delta t C_{67-} \left( k + \frac{1}{2} \right) \frac{1}{4} [E_z(i, j, k+1) + E_z(i, j, k)] [u_6(i, j, k+1) + u_6(i, j, k)], \\
u_8(i, j, k+1) &= u_8(i, j, k) + \Delta t C_{68-} \left( k + \frac{1}{2} \right) \frac{1}{4} [E_z(i, j, k+1) + E_z(i, j, k)] [u_6(i, j, k+1) + u_6(i, j, k)].
\end{aligned} \tag{A6}$$

In order to obtain values for the electric-field components and material variables at mesh points where they are not defined, the following averaging procedure is performed:

$$\begin{aligned}
E_y \left( i + \frac{1}{2}, j \right) &= \frac{1}{4} \left[ E_y \left( i + \frac{1}{2}, j - \frac{1}{2} \right) + E_y \left( i + 1, j + \frac{1}{2} \right) \right. \\
&\quad \left. + E_y \left( i, j - \frac{1}{2} \right) + E_y \left( i, j + \frac{1}{2} \right) \right],
\end{aligned}$$

$$\begin{aligned}
E_z \left( i, j + \frac{1}{2} \right) &= \frac{1}{4} \left[ E_z \left( i + \frac{1}{2}, j \right) + E_z \left( i + \frac{1}{2}, j + 1 \right) \right. \\
&\quad \left. + E_z \left( i - \frac{1}{2}, j \right) + E_z \left( i - \frac{1}{2}, j + 1 \right) \right],
\end{aligned}$$

$$u_l \left( i, j + \frac{1}{2} \right) = \frac{1}{2} [u_l(i, j) + u_l(i, j+1)],$$

$$u_l \left( i + \frac{1}{2}, j \right) = \frac{1}{2} [u_l(i, j) + u_l(i+1, j)] \quad (l=1,2,\dots,8),$$

$$E_y(i, j) = \frac{1}{2} \left[ E_y \left( i, j - \frac{1}{2} \right) + E_y \left( i, j + \frac{1}{2} \right) \right],$$

$$E_z(i, j) = \frac{1}{2} \left[ E_z \left( i + \frac{1}{2}, j \right) + E_z \left( i - \frac{1}{2}, j \right) \right]. \tag{A7}$$

From inspection of Eq. (A5a), it can be seen that the magnetic field is updated at a time different from the other terms in the system, and therefore it is advanced in the stan-

dard leapfrog way. For the rest of the equations we apply a predictor-corrector method, casting the system in the form

$$W_i^{\text{new}} = W_i^{\text{old}} + \Delta t F_i(\tilde{W}^{\text{old}}, \tilde{W}^{\text{new}}) \quad \text{for } i=1,2,\dots,10, \quad (\text{A8})$$

where  $W_1 = E_y$ ,  $W_2 = E_z$ ,  $W_3 = U_1$ ,  $W_4 = U_2, \dots$ ,  $W_{10} = U_8$ , and the functionals  $F_i$  represent the terms at the right-hand sides of Eqs. (A5b), (A5c), and (A6) combined with the common multiplier, the time step  $\Delta t$ . The coefficients in  $F_i$  are updated, and initially the new values  $\tilde{W}^{\text{new}}$  are set equal to their values in the previous time step  $\tilde{W}^{\text{old}}$ , thus giving the

updated values  $\tilde{W}_i^{\text{new}}$  from Eq. (A8). These values are compared with the values of  $\tilde{W}^{\text{new}}$  before updating using Eq. (A8), and the iterative procedure continues until the difference becomes smaller than a specified value. Typically, the process converges quickly enough to give a difference of  $10^{-5}$  between the previous and new values of  $\tilde{W}^{\text{new}}$ . The updated values for the pseudospin vector components are obtained from Eq. (A1).

The predictor-corrector iterative scheme described above has proved to be stable and computationally efficient for large spatial arrays (e.g.,  $60\,000 \times 100$  grid points).

- 
- [1] M. Nisoli, S. De Silvestri, O. Svelto, R. Szipocs, K. Ferencz, Ch. Spielmann, S. Sartania, and F. Krausz, *Opt. Lett.* **22**, 522 (1997).
- [2] A. Baltuska, Z. Wei, M. S. Pshenichnikov, and D. A. Wiersma, *Opt. Lett.* **22**, 102 (1997).
- [3] V. P. Kalosha, M. Müller, and J. Herrmann, *J. Opt. Soc. Am. B* **16**, 323 (1999).
- [4] P. Michler, A. Lohner, W. W. Rühle, and G. Reiner, *Appl. Phys. Lett.* **66**, 1599 (1995).
- [5] G. Pompe, T. Rappen, and M. Wegener, *Phys. Rev. B* **51**, 7005 (1995).
- [6] F. Jahnke, H. C. Schneider, and S. W. Koch, *Appl. Phys. Lett.* **69**, 1185 (1996).
- [7] S. Hughes, *Phys. Rev. Lett.* **81**, 3363 (1998).
- [8] A. V. Tarasishin, S. A. Magnitskii, V. A. Shuvaev, and A. M. Zheltikov, *Opt. Express* **8**, 452 (2001).
- [9] R. W. Ziolkowski, J. M. Arnold, and D. M. Gogny, *Phys. Rev. A* **52**, 3082 (1995).
- [10] G. Slavcheva, J. M. Arnold, and I. Wallace, in *Proceedings of The 15th Quantum Electronics and Photonics Conference*, (Institute of Physics, Glasgow, 2001).
- [11] F. de Rougemont and R. Frey, *Phys. Rev. B* **37**, 1237 (1988).
- [12] B. Thédrez, A. Jones, and R. Frey, *IEEE J. Quantum Electron.* **24**, 1499 (1988).
- [13] C. M. Bowden and G. P. Agrawal, *Phys. Rev. A* **51**, 4132 (1995).
- [14] F. T. Hioe and J. H. Eberly, *Phys. Rev. Lett.* **47**, 838 (1981).
- [15] F. T. Hioe and J. H. Eberly, *Phys. Rev. A* **25**, 2168 (1982).
- [16] F. T. Hioe, *Phys. Rev. A* **28**, 879 (1983).
- [17] R. P. Feynman, F. L. Vernon, and R. W. Hellwarth, *J. Appl. Phys.* **28**, 49 (1957).
- [18] R. J. Cook and B. W. Shore, *Phys. Rev. A* **20**, 539 (1979).
- [19] J. N. Elgin, *Phys. Lett.* **80A**, 140 (1980).
- [20] P. K. Aravind, *J. Opt. Soc. Am. B* **3**, 1025 (1986).
- [21] M. Gell-Mann and Y. Neeman, *The Eightfold Way* (Benjamin, New York, 1964).
- [22] K. S. Yee, *IEEE Trans. Antennas Propag.* **14**, 302 (1966).
- [23] B. Engquist and A. Majda, *Math. Comput.* **31**, 629 (1977).
- [24] G. Mur, *IEEE Trans. Electromagn. Compat.* **23**, 377 (1981).
- [25] A. Taflov, *Computational Electrodynamics: The Finite-Difference Time-Domain Method* (Artech House, Norwood, MA, 1995).
- [26] M. J. Adams, *An Introduction to Optical Waveguides* (Wiley, New York, 1981), p. 7.
- [27] S. L. McCall and E. L. Hahn, *Phys. Rev.* **183**, 457 (1969).
- [28] S. L. McCall and E. L. Hahn, *Phys. Rev. Lett.* **18**, 908 (1967).
- [29] R. K. Dodd, J. C. Eilbeck, J. D. Gibbon, and H. C. Morris, *Solitons and Nonlinear Wave Equations* (Academic, London, 1994).